Nature Communications

https://doi.org/10.1038/s41467-026-69545-3

Article in Press

# Spatiotemporal interplay between epithelial and mesenchymal cells drives human dentinogenesis

Received: 21 May 2025

Accepted: 4 February 2026

Cite this article as: Wei, W., Wu, C., Sun, J. *et al.* Spatiotemporal interplay between epithelial and mesenchymal cells drives human dentinogenesis. *Nat Commun* (2026). https://doi.org/10.1038/s41467-026-69545-3

**Wei Wei, Chuan Wu, Jing Sun, Mengjie Han, Xiuge Gu, Hanzhang Zhou, Xiaoshan Wu, Zongshan Shen, Chunmei Zhang, Jinsong Wang, Lei Hu, Lanrong Luo, Yuanyuan Zhang, Lina Hu, Songlin Wang & Ran Zhang**

# Spatiotemporal Interplay Between Epithelial and Mesenchymal Cells Drives Human Dentinogenesis

Wei Wei[1†], Chuan Wu[1†], Jing Sun[1], Mengjie Han[2], Xiuge Gu[1], Hanzhang Zhou[2], Xiaoshan Wu[1,3], Zongshan Shen[1,4], Chunmei Zhang[1], Jinsong Wang[5], Lei Hu[1], Lanrong Luo[6], Yuanyuan Zhang[6], Lina Hu[6], Songlin Wang[1,3,7*], Ran Zhang[1,2*]

[1]Laboratory of Oral Health and Homeostatic Medicine, School of Stomatology and Beijing Stomatological Hospital and Beijing Laboratory of Oral Health, Capital Medical University, Beijing 100070, China

[2]Department of Oral Pathology, Peking University School and Hospital of Stomatology & National Center of Stomatology & National Clinical Research Center for Oral Diseases & National Engineering Research Center of Oral Biomaterials and Digital Medical Devices, Beijing, 100081, China

[3]Academician Workstation for Oral-Maxillofacial Regenerative Medicine, Central South University, Changsha, 410008, China

[4]Hospital of Stomatology, Guangdong Provincial Key Laboratory of Stomatology, Guanghua School of Stomatology, Sun Yat-sen University, Guangzhou, 510055, China

[5]Department of Biochemistry and Molecular Biology, School of Basic Medical Sciences, Capital Medical University, Beijing, 100069, China

[6]Department of Reproductive Regulation, Beijing Obstetrics and Gynecology Hospital, Beijing Maternal and Child Health Care Hospital, Capital Medical University, 100026, Beijing, China

[7]Laboratory of Homeostatic Medicine, School of Medicine, Southern University of Science and Technology, Shenzhen, 518055, China

[†]Wei Wei and Chuan Wu contributed equally to this article.

*Correspondence: rani@bjmu.edu.cn; slwang@ccmu.edu.cn



## ABSTRACT

Tooth dentin, secreted by odontoblasts, constitutes most of the tooth structure and provides support and sensory function. However, dentin defects are common and irreparable once they exceed a critical threshold. Human dentin develops from dental papilla (DP) cells under the guidance of the dental epithelium (DE). Here, we present a human tooth development atlas from initiation to erupted stage using single-cell RNA sequencing and spatial transcriptomics, focusing on epithelial-mesenchymal interactions. This atlas reveals that DE orchestrates DP differentiation in a WNT-NOTCH sequential activation model and identifies the key signaling molecules. *DLX6-AS1*$^{+}$ DP cells respond to dental epithelial signals and can be isolated

from adult dental pulp stem cells (DPSCs). Notably, *DLX6-AS1*$^{+}$ DPSCs successfully generate tubular dentin in an *in vivo* disease model of dentin defects. This research provides valuable information on human tooth development and establishes a basis for repairing regenerative dental tissue.

**KEYWORDS**

WNT signaling, NOTCH signaling, dentin regeneration, single-cell RNA sequencing, spatial transcriptomics

## INTRODUCTION

Dental hard tissues comprise enamel, dentin, and cementum, with dentin forming the primary structural component of teeth. Produced by odontoblasts, dentin provides mechanical support and sensory function essential for tooth integrity[1]. Pathological conditions such as dental caries trigger odontoblast apoptosis[2], prompting the pulp to form reparative dentin as a protective barrier. However, aging or chronic inflammation impair this regenerative capacity[3]. Understanding the cellular origin and molecular mechanisms underlying dentin development and regeneration remains a critical challenge.

During organogenesis, the orchestrated regulation of conserved signaling pathways governs cell fate determination, proliferation, and differentiation. Tooth development, a paradigm of ectoderm-derived organogenesis, exemplifies such complexity. Congenital genetic diseases such as dentinogenesis imperfecta can lead to dentin loss, along with injuries and damage[4]. Additionally, patients with ectodermal dysplasia frequently exhibit dentin loss and deformities due to epithelial cell dysfunction[5]. The development and homeostasis of dental tissues depend on reciprocal interactions between dental epithelium (DE) and dental mesenchyme derived tissues, such as dental papilla (DP), which collectively determine tooth morphology, dimensions, and functional integrity[6, 7, 8]. Within this interaction network, dental epithelial signals guide some DP cells to differentiate into odontoblasts, while others remain undifferentiated in adult pulp, serving as a reservoir for reparative dentin formation upon pulp exposure. This highlights the importance of DE signaling in determining DP cell fate. Our recent research has shown the crucial role of DE in early human tooth development[9], but further studies are needed to understand how DE guides odontoblast differentiation throughout tooth development from initiation to erupted stage and whether these signals could be utilized in tooth regeneration.

Molecular studies have revealed that multiple signaling cascades, including WNT[10, 11], NOTCH[12], BMP[13, 14], TGF-β[15], and FGF[16, 17], orchestrate epithelial-mesenchymal interactions during tooth development. However, the precise mechanisms governing these interactions in human odontogenesis remain to be fully elucidated. In particular, DE-derived WNT signals initiate mesenchymal cell proliferation and differentiation, as demonstrated in mouse models where disruption of epithelial WNT secretion impairs odontoblast differentiation[18, 19]. The NOTCH signaling system, through its classical roles in cell fate determination via

ligand-receptor interactions between adjacent cells, contributes to tooth development[20, 21]. These molecular networks work together rather than separately, creating a complex regulatory system, yet the spatiotemporal regulation network of these crucial signaling pathways still needs to be explored[22]. The WNT-NOTCH signaling axis has emerged as a critical regulator of progenitor cell maintenance, terminal differentiation, and regeneration in human tissues[23, 24]. However, its precise operational mode in human tooth development and regeneration requires further elucidation. This understanding is particularly crucial given that odontogenic stem cells in monophyodont rodents exhibit distinct functional characteristics from their human counterparts[25], necessitating human-specific investigations into tooth development and regeneration mechanisms.

To advance our understanding of human tooth structures, we established a comprehensive developmental atlas of human teeth from initiation to erupted stage using integrated single-cell RNA sequencing (scRNA-seq) and spatial transcriptomics (ST). By mapping the interactions between ligands and receptors of tooth-related signaling molecules, we identified key DE-derived molecules that play a crucial role in directing DP differentiation. Functional validation revealed their dentinogenic superiority over controls. Moreover, we identified previously unknown subgroups of dental pulp stem cells (DPSCs); notably, these subgroups can regenerate dentin to repair dentin defects, as demonstrated in a relevant animal model. These results not only progress our insights into human development, but also present a blueprint for regenerative solutions.

## RESULTS

### Spatiotemporal cellular dynamics and molecular regulation in tooth development

To construct a comprehensive developmental timeline of human tooth formation, we collected and analyzed scRNA-seq and ST data spanning multiple developmental stages, from initiation to erupted stage[9, 25, 26, 27, 28] (Fig. 1a). Following quality control and integration of scRNA-seq data, we performed systematic cell type classification and marker gene identification to establish a tooth developmental atlas. Uniform Manifold Approximation and Projection (UMAP) analysis revealed 11 cell clusters and their temporal distribution patterns (Fig. 1b and Supplementary Fig. 1a). Cell populations were identified based on canonical marker gene expression: DE (*KRT19*, *KRT5*, *KRT14*), DP lineage (DPL) (*FGF3*, *RSPO4*, *DLX6-AS1*), and dental follicle (DF) (*COL12A1*, *POSTN*, *OGN*). Endothelial cells (*ESAM*, *CLDN5*, *VWF*), fibroblasts (*PDGFRB*, *RGS5*, *BGN*), monocytes (*TYROBP*, *AIF1*, *CD14*), lymphocytes (*TRBC2*, *CD3E*, *CD48*), erythroblasts (*ALAS2*, *HBG1*, *HBA1*), vascular smooth muscle cells (*ACTC1*, *SGCA*, *TNNT1*), and neuronal cells (*S100B*, *MPZ*, *PLP1*) were defined according to their specific markers[9, 26, 29] (Fig. 1c). The consistent expression patterns of key markers were observed across all batches, as depicted in both FeaturePlots and violin plots (VlnPlots) (Supplementary Fig. 1b). A detailed list of the top 10 differentially expressed genes defining each

major cell lineage can be found in Supplementary Fig. 2a. Integration of scRNA-seq and ST analyses provided detailed insights into the spatial distribution and gene expression profiles of two key cell populations: DE and DPL (Fig. 1d). Spatial heatmap analysis and immunofluorescence (IF) staining further validated our cell clustering approach (Fig. 1e). KRT14 specifically labeled the DE, while *FGF3* was localized to the DPL, as illustrated in Fig. 1e. To confirm the specificity of these signals, co-staining was performed with the differentiation markers *AMELX* (for DE) and DSPP (for DPL). Isotype negative controls demonstrated the absence of non-specific signals (Supplementary Fig. 2b).

To understand the molecular mechanisms involved in human tooth development, we analyzed the expression patterns of key developmental signaling pathways in DE and DPL. We isolated DE and DPL cell populations and identified genes related to ligands and receptors from signaling pathways crucial for tooth development, such as WNT, NOTCH, BMP/TGF-β, FGF, SHH, and EDA signaling pathways[6]. We examined the expression levels of these genes in the two cell populations, calculated the total expression of each signaling pathway, and represented the data in pie charts to show the expression proportions of each pathway in DE and DPL (Fig. 1f). Our analysis revealed that WNT (*WNT1*/*3A*/*4*/*5A*/*5B*/*6*/*7A*/*7B*/*8B*/*10A*/*10B*/*11*), NOTCH (*JAG1*/*2*, *DLL1*/*3*/*4*), SHH (*SHH*, *IHH*, *DHH*), and EDA ligands were predominantly expressed in DE, while their corresponding receptors were mainly expressed in DPL. Conversely, BMP (*BMP2*/*3*/*4*/*5*/*6*/*7*/*10*/*15*), TGF-β (*TGF-β1*/*2*/*3*), and FGF (*FGF2*/*3*/*8*/*10*) ligands showed higher expression levels in DPL. Detailed gene-level statistics and absolute expression values are provided in Supplementary Data 1. Moreover, to evaluate the functional significance of these pathways, pathway activity scoring was conducted. The results indicated increased activity in the EDA pathway in DE and in the BMP, TGF-β, and FGF pathways in DPL, suggesting their specific roles within each lineage (Supplementary Fig. 2c).

ScRNA-seq data revealed that WNT and NOTCH ligands were main signals secreted by the DE throughout all developmental stages. However, their relative abundance varied at different stages. In early stages, WNT ligand expression was predominant while NOTCH ligand expression was low. As development progressed, there was a shift towards increased NOTCH expression and decreased WNT expression (Fig. 1g). The overall activity of key signaling pathways was further assessed across various time points (Supplementary Fig. 2d). Consistent with the trend shown in Fig. 1g, the WNT and NOTCH pathways exhibited a relay-like dynamic during development, whereas the SHH pathway maintained activity throughout the 12-24 (post-conception week, PCW) period. The BMP and TGF-β pathways displayed sustained expression throughout all stages of development. To investigate interaction details at specific time points, we focused on the 15-17 PCW window, utilizing CellChat to predict signaling communication between DE and DPL cells. At 17 PCW, the NOTCH pathway showed robust interaction, predominantly initiated by DE cells and directed towards DPL cells, suggesting a mechanism of epithelial-to-mesenchymal

NOTCH signaling (Supplementary Fig. 2e-g). The integrated analysis of scRNA-seq and ST data indicated that the human DE orchestrated DPL development by regulating multiple developmental pathways in a coordinated manner. This initial analysis laid the groundwork for our subsequent hypothesis, which was then substantiated through further validation.

**Temporal and spatial orchestration of WNT and NOTCH signaling during tooth development**

Analysis of scRNA-seq data revealed that WNT and NOTCH pathways components were not only predominantly expressed by DE but also exhibited distinct temporal expression patterns during tooth development. To delineate the relationship between these pathways, we performed comprehensive analyses using scatter plots and pie charts. Notably, the gene expression of WNT family ligands showed tissue specificity. Ligands associated with the canonical WNT/β-catenin pathway[30], such as *WNT1*, *WNT3A*, *WNT4*, *WNT8B*, *WNT10A*, and *WNT10B* were predominantly expressed in the DE. In the non-canonical WNT pathway[31], *WNT5A*, *WNT5B*, *WNT6*, *WNT7A*, *WNT7B*, and *WNT11* exhibited distinct distribution patterns. Specifically, *WNT6*, *WNT7A*, and *WNT7B* were predominantly expressed in the DE, while *WNT5A*, *WNT5B*, and *WNT11* showed higher levels of expression in the DPL. The sequencing data revealed that the DE was the primary source of NOTCH pathway components *JAG1* and *JAG2* (Fig. 2a).

Temporal analysis using bubble heatmap visualization uncovered a unique "relay" mechanism between the WNT and NOTCH signaling pathways in tooth development. In the early stages (7-15 PCW), the DE exhibited high expression of WNT ligands, while the DPL displayed elevated expression of WNT receptors. However, post 15 PCW, WNT ligand expression declined, accompanied by a rise in NOTCH ligand expression in DE, NOTCH receptor expression in DPL, and WNT antagonist expression in DPL (Fig. 2b). To gain a deeper insight into the possible cellular crosstalk, we analyzed the temporal dynamics of ligands in DPL and their corresponding receptors in DE (Supplementary Fig. 3a). Our analysis suggested a potential autocrine/paracrine regulatory loops within the DE. Fig. 2c displayed the most prominently expressed WNT and NOTCH ligands in DE based on previous sequencing data. To distinguish the potential activities of canonical versus non-canonical WNT signaling, we plotted the expression profile for each ligand individually (Supplementary Fig. 3b). This analysis revealed dynamic expression patterns for each ligand, suggesting a spatiotemporal regulation of different signaling activities during DE development. To investigate the heterogeneity within the DE, we performed a detailed sub-clustering analysis, identifying several subpopulations (Supplementary Fig. 3c). Each subpopulation was characterized by a distinct molecular signature based on its top differentially expressed genes[9] (Supplementary Fig. 3d). Notably, FeaturePlots revealed highly specific expression patterns of key signaling ligands： *WNT6*, *WNT7B* and *JAG1* were predominantly expressed in the outer enamel epithelium (OEE), cervical loop (CL), inner enamel epithelium (IEE), and enamel knot (EK). *WNT10B* expression was specifically localized to the EK

(Fig. 2d and Supplementary Fig. 3e). We conducted ST mapping of the key molecules identified in Fig. 2c to spatially validate the findings, offering detailed insights into their tissue distribution patterns (Supplementary Fig. 3f). To validate our transcriptomic findings at the protein level, we performed IF staining. This analysis not only verified the precise protein localization (Fig. 2d) but also illustrated the activation of pathways by showing robust expression of the downstream targets LEF1[32] and HEY1[33]. The subsequent quantification of these signals further emphasized the complex spatiotemporal coordination of WNT and NOTCH signaling during human tooth development (Supplementary Fig. 3g).

**_DLX6-AS1_$^+$ DP cells exhibit a specific expression pattern in human fetal teeth and potentially receive WNT-NOTCH signaling from the DE**

In our recent study, we classified DP cells in the early stage into two subpopulations according to their location[9]. By incorporating late-stage data, we further subclustered DPL cells into three clusters: *DLX6-AS1*$^+$ DP, odontoblasts and *NR2F1*$^+$*TWIST1*$^+$ DP based on their markers and developmental trajectory analysis[34] (Fig. 3a-b). Histograms were generated to assess the temporal stability of distinct fates by categorizing cells according to their developmental stage and key marker genes (Supplementary Fig. 4a). *DLX6-AS1*$^+$ DP cells, characterized by high *DLX6-AS1* expression, were located in close proximity to DE cells (Fig. 3c-d). In mice, the expression of *Dlx6os1*, the murine homolog of human *DLX6-AS1*, showed minimal expression in the mouse molar at E16.5, a stage coinciding with the emergence of CDP in mice[35], suggesting distinctive developmental markers and patterns in human tooth development (Supplementary Fig. 4b-c).

Based on the analysis of their location and trajectory analysis, we proposed that *DLX6-AS1*$^+$ DP cells may be responsive to DE signals and act as potential progenitors for odontoblasts (Fig. 3d). To investigate this hypothesis, differential gene expression analysis was conducted to characterize the molecular signatures of *DLX6-AS1*$^+$ and *NR2F1*$^+$*TWIST1*$^+$ DP cells, revealing different transcriptomic profiles for each subpopulation (Fig. 3e). Pathway enrichment analysis on the upregulated genes in each group was performed to computationally investigate potential functional consequences, supporting the hypothesis of a functional divergence between the two subpopulations (Supplementary Fig. 4d). We found increased expression of *LEF1* and *HEY1*, which are target genes of the WNT and NOTCH signaling pathways respectively, in the *DLX6-AS1*$^+$ DP cells (Fig. 3e). Key receptors and target genes of WNT and NOTCH signaling pathways were confirmed through scRNA-seq and ST data (Fig. 3f and Supplementary Fig. 4e).

The temporal gene expression profile of *DLX6-AS1*$^+$ DP cells indicated distinct gene expression patterns at different time points. Early-stage genes such as *MEIS2* and *TFAP2B* were linked to the WNT signaling pathway, while late-stage genes like *ZBTB16* were associated with the NOTCH signaling pathway (Fig. 3g). A comparison of scRNA-seq data from 15 PCW and 17 PCW further illustrated this transition via volcano

plot. *DLX6-AS1*$^+$ DP cells of 15 PCW exhibited upregulated *EGR1* and *FOXO1* expression, which are related to the WNT signaling pathway, while *DLX6-AS1*$^+$ DP cells of 17 PCW showed increased expression of *HEY1* and *IFITM5*, which are associated with the NOTCH signaling pathway (Fig. 3g). Furthermore, the expression patterns of WNT, NOTCH, and odontogenesis-related genes were compared between *DLX6-AS1*$^+$ DP cells and *NR2F1*$^+$*TWIST1*$^+$ DP cells using ST data (Supplementary Fig. 4f). Correlation analysis revealed a positive co-expression between *DLX6-AS1* and odontogenesis-related molecules[36, 37], including *DLX1*, *BMP4*, *RUNX2*, *DSPP* and *DMP1*, and WNT/NOTCH pathway components, such as *LEF1, LRP5*, *NOTCH2* and *HEY1* (Fig. 3h). The role of *DLX6-AS1* in odontogenesis was indicated in our recent study[38] as well as in other research[39].

**Application of WNT-NOTCH signaling in odontogenic differentiation of *DLX6-AS1*$^+$ cells**

*DLX6-AS1*$^+$ DMSCs and DPSCs, representing different differentiation statuses of DP cells, were isolated using a lentiviral reporter system with the *DLX6-AS1* promoter-driven EGFP to investigate their odontogenic potential and suitability as seed cells for dentin regeneration. A negative control group was included by transducing cells with an empty lentiviral vector (Supplementary Fig. 5a-d). Both experimental and control groups underwent puromycin selection *in vitro*. *DLX6-AS1*$^+$ DMSCs exhibited elevated expression of the odontoblast differentiation marker DSPP, as well as the WNT/NOTCH target genes LEF1 and HEY1, after a 21-day odontogenic induction (Fig. 4a), consistent with the gene signatures identified in precious analysis. Alkaline phosphatase (ALP) and Alizarin red S (ARS) staining confirmed our observations, showing enhanced odontogenic differentiation in *DLX6-AS1*$^+$ DMSCs (Fig. 4b). Next, we assessed whether a WNT-NOTCH sequential treatment could enhance the odontogenic potential of *DLX6-AS1*$^+$ DMSCs and *DLX6-AS1*$^+$ DPSCs. Using scRNA-seq and ST data, we developed a protocol for odontoblast differentiation. *DLX6-AS1*$^+$ DMSCs were initially cultured in a medium supplemented with WNTs (WNT6, WNT7B, and WNT10B at a concentration of 10 ng/ml) from day 1 to day 7. Subsequently, on day 8, the culture medium was changed to one containing JAG1 (at 10 ng/ml), which was maintained until day 14. The growth factor-supplemented medium was refreshed every two days throughout the induction period to ensure continuous stimulation, as indicated by increased expression of target genes for both pathways in the western blot analysis (Fig. 4c). By day 21, an enhancement in odontogenic differentiation was observed in the group subjected to sequential WNT-NOTCH stimulation, as evidenced by ALP and ARS staining (Fig. 4d). Our findings, detailed in Supplementary Fig. 5e, show that the sequential WNT-NOTCH stimulation leads to a significantly higher level of mineralization compared to the conventional odontogenic induction protocol. IF staining showed increased expression of odontogenic markers DSPP and KI67 in this group (Fig. 4e). Additionally, WNT-NOTCH sequential stimulation upregulated *DLX6-AS1* expression in DMSC (Supplementary Fig. 5f). To confirm our analysis that epithelial-derived WNT-NOTCH signaling directed DP

odontogenic differentiation, we established a co-culture system with DE and *DLX6-AS1*$^+$ DMSCs. When we inhibited WNT and NOTCH signaling from DE cells, we observed decreased expression of odontogenic markers *DMP1* and *DSPP* in the *DLX6-AS1*$^+$ DMSCs (Fig. 4f). These findings underscored the importance of DE-derived WNT-NOTCH signaling in DP differentiation.

DPSCs, a type of mesenchymal stem cells, are easily obtained from extracted third molars or exfoliated deciduous teeth. Their low immunogenicity makes them suitable candidates for both autologous and allogeneic therapeutic applications. Our group has conducted extensive research on DPSC-based therapies[40, 41], leading to their advancement to phase I clinical trial and investigator-initiated trial. DPSCs have the potential to differentiate into odontoblasts for pulp-dentin complex regeneration[42], but enhancing their dentinogenic inducing ability is a key challenge that needs to be addressed. Advances in differentiation and selection protocols could contribute to making DPSCs more effective in clinical applications. We applied the same WNT-NOTCH sequential stimulation on *DLX6-AS1*$^+$ DPSCs and observed significantly enhanced odontogenic differentiation effects in the WNT-NOTCH sequential stimulation group (Fig. 4g-j).

**Utilizing sequential WNT-NOTCH signaling in a recombinant model promotes dentinogenesis**

To validate the odontogenic differentiation of *DLX6-AS1*$^+$ cells mediated by WNT-NOTCH signal i*n vivo*, we utilized a tissue recombinant strategy. DMSCs or *DLX6-AS1*$^+$ DMSCs were combined with non-dental human keratinocytes and transplanted beneath the renal capsule. In the Pre-WNTs+JAG1 treatment group, *DLX6-AS1*$^+$ DMSCs were pre-treated with WNTs (WNT6, WNT7B and WNT10B) before being combined with keratinocytes to replicate the developmental signaling milieu. JAG1-soaked beads, as pre-established protocols[43], were transplanted in close proximity to the recombinants (Fig. 5a).

Histological analysis was conducted to evaluate the recombinants under different treatment conditions. Hematoxylin and Eosin (H&E) staining revealed the overall tissue organization and morphological features (Supplementary Fig. 6a). Masson's Trichrome staining was employed to assess extracellular matrix composition, tissue fibrosis, and collagen fiber arrangement (Fig. 5b). Among all experimental groups, only the recombinants from the *DLX6-AS1*$^+$ DMSCs with Pre-WNTs+JAG1 treatment group generated tooth-like structures, characterized by finely deposited pre-dentin and dentin of tubular structure arranged parallel to each other. DSPP, a marker for odontoblast differentiation, was employed to evaluate differentiation in the recombinants (Fig. 5c). The expression of these proteins indicated functional and structural maturation of odontoblasts. Notably, the recombinants from *DLX6-AS1*$^+$ DMSCs with Pre-WNTs+JAG1 treatment group showed significantly upregulated expression of the odontogenic marker DSPP, as confirmed by quantitative analysis (Fig. 5c and Supplementary Fig. 6b). The specificity of this staining was confirmed with an isotype control, which showed only negligible background fluorescence (Supplementary Fig. 6c). To confirm that the transplanted cells were responsible for this new tissue formation, we tracked GFP-labeled *DLX6-AS1*$^+$

DMSCs. Indeed, these GFP-positive cells (green) were observed to be actively secreting DSPP (red), directly linking our target cell population to the process of dentinogenesis (Fig. 5e). We also assessed Micro-CT analysis of the recombinants by evaluating its mineralization. Micro-CT analysis revealed the formation of robust mineralized tissue in the recombinants from the *DLX6-AS1*$^+$ DMSCs with Pre-WNTs+JAG1 treatment group (Fig. 5d).

In conclusion, only the WNT-NOTCH sequential stimulation was capable of directing *DLX6-AS1*$^+$ DMSCs towards generating dentin-like structures *ex vivo*, showing the therapeutic potential of *DLX6-AS1*$^+$ DMSCs under WNT-NOTCH sequential stimulation for applications in dental tissue and other ectodermal-derived organ engineering.

**Repair of dentin defects by *DLX6-AS1*$^+$ DPSCs using the sequential application of WNT-NOTCH signaling**

With the ongoing clinical trials of DPSC as a promising cell type for clinical applications, we next investigate the dentin regeneration capacity of *DLX6-AS1*$^+$ DPSCs by establishing a nude mouse molar tooth injury model. *DLX6-AS1*$^+$ DPSCs were isolated from extracted third molars and were pre-treated with WNTs (WNT6, WNT7B and WNT10B), then injected into the pulp exposure site along with JAG1 (Fig. 6a). This intervention showed no adverse effects on vital organs, including the liver, spleen, and kidneys (Supplementary Fig. 7a-c). With the assistance of micro-CT analysis, it was clearly demonstrated that the *DLX6-AS1*$^+$ DPSCs treated with WNT-NOTCH sequential stimulation could promote dentin regeneration (Fig. 6b). Quantitative analysis verified a notable increase in mineralized tissue volume fraction (BV/TV) and tissue mineral density (TMD) at the damage sites compared to the controls (Fig. 6c). 28 days post-injury, histological assessment was performed using Masson's Trichrome staining and IF analysis. The results showed that in the group treated with *DLX6-AS1*$^+$ DPSCs receiving WNT-NOTCH sequential stimulation, a dentine bridge was formed at the damaged site of the mouse molar (Fig. 6d). In contrast to the disorganized pattern typically seen in reparative dentin, our regenerated dentin exhibited a well-arranged tubular structure, as indicated by the arrows in the zoomed-in image. Expression of DSPP was detected beneath the dentine bridge in the group treated with *DLX6-AS1*$^+$ DPSCs receiving WNT-NOTCH sequential stimulation (Fig. 6d). SEM analyses showed that the tissue developed in the *DLX6-AS1*$^+$ DPSCs with WNT-NOTCH sequential stimulation group exhibited a well-organized, tubular ultrastructure resembling natural dentin (Fig. 6d). qPCR results indicated that the molars treated with *DLX6-AS1*$^+$ DPSCs receiving WNT-NOTCH sequential stimulation highly expressed *DMP1*, *ALP*, and *MEPE* (Fig. 6e). Notably, using the co-labeling of human *DLX6-AS1* and DSPP proteins with RNA scope technology, it was shown that human *DLX6-AS1*$^+$ DPSCs (red-stained) were arranged in a single row on the side close to the regenerated dentin. Strong DSPP expression was observed in these well-arranged *DLX6-AS1*$^+$ DPSCs,

indicating their ability to differentiate into regenerative odontoblasts (Fig. 6f). IF analysis confirmed the origin of the reparative dentin from the transplanted progenitors, demonstrating GFP-labeled *DLX6-AS1*$^+$ DPSCs co-expressing the odontoblast marker DSPP within the newly formed matrix (Supplementary Fig. 7d). These findings demonstrate the potential of developmentally-guided *DLX6-AS1*$^+$ DPSCs for therapeutic dentin regeneration, offering a strategy for utilizing discarded dental pulp tissue. A model for odontoblast differentiation and regeneration was established based on previous analysis and studies. During tooth development, undifferentiated ectomesenchymal cells in the dental pulp divide under the influence of WNT signals from the DE to become *DLX6-AS1*$^+$ DP cells. One daughter cell differentiates into an odontoblast in response to NOTCH signals from the DE, while the other daughter cell remains as a subodontoblast cell. *DLX6-AS1*$^+$ DPSCs can be isolated and, when exposed to sequential WNT-NOTCH signaling, can generate human dentin in dentin defects (Fig. 6g).

## DISCUSSION

During organogenesis, the meticulous coordination of signaling pathways plays a crucial role in tissue morphogenesis and functional specialization. The compartmentalized expression of signaling ligands and receptors between the DE and DM underscores the significance of epithelial-mesenchymal interactions in tooth development[23, 44]. Our findings demonstrated that WNT and NOTCH ligands were predominantly expressed in the DE, whereas their receptors were localized in the DP. This spatial distribution pattern aligned with previous reports that have emphasized the instructive role of epithelial-derived signals in mesenchymal differentiation during organogenesis[45, 46, 47, 48]. Furthermore, our temporal analysis delineated a "relay" mechanism: WNT signaling predominated in the early stages, initiating mesenchymal proliferation and differentiation. Subsequently, NOTCH signaling became prominent after 15 PCW, potentially optimizing cell fate determination and maintaining odontoblast lineage commitment. Notably, the expression of WNT antagonists in the DP during later stages may function as a feedback loop to attenuate WNT activity[49, 50], thereby facilitating the transition to NOTCH-dependent regulation. This dynamic regulation ensures precise control over differentiation timing and prevents premature or ectopic mineralization - a critical feature given the spatial constraints of tooth morphogenesis. Although the precise molecular mechanisms governing this transition require further investigation, this sequential activation pattern appears to be essential for normal odontogenic differentiation.

Our analyses suggested *DLX6-AS1*$^+$ cells as key responders to epithelial WNT-NOTCH signaling. These cells were strategically positioned in the coronal papilla adjacent to the epithelium, facilitating the reception of spatial signals. Trajectory analysis demonstrated that *DLX6-AS1*$^+$ cells exhibited characteristics of odontoblast priming. Pathway enrichment and co-expression analyses revealed that *DLX6-AS1*$^+$ cells displayed a distinctive response to WNT-NOTCH signaling. This molecular signature

correlated with enhanced mineralization capacity *in vitro* and the formation of dentin-like structures *in vivo*. The sequential activation pattern, whereby WNT signaling (mediating proliferation/priming)[51, 52] preceded NOTCH signaling (governing differentiation/specification)[52, 53], aligned with their established roles in orchestrating odontoblast maturation. We observed that this initial proliferative phase occurred concurrently with the upregulation of DSPP, suggesting that the expansion of the progenitor pool could be a prerequisite for generating a sufficient cell population for functional maturation. Importantly, our co-culture experiments demonstrated that epithelial-derived signals were essential for this process, as WNT-NOTCH signaling inhibition abolished their odontogenic potential. While our previous study suggested the functional necessity of *DLX6-AS1* for odontogenic differentiation[38], the current study helps to bridge a gap by suggesting that *DLX6-AS1* may be a component for integrating the WNT-NOTCH signaling axis. Our preliminary transcriptomic analysis revealed that the cellular response to WNT/NOTCH stimulation was impaired in the absence of *DLX6-AS1*, and molecular docking simulations further suggested a potential binding interface with LEF1, collectively positioning *DLX6-AS1* as a target for promoting dentin-pulp complex regeneration.

While the epithelium predominantly secretes WNT and NOTCH ligands, the signaling landscape of epithelial-mesenchymal axis during tooth development is far more complex. Our data also showed WNT and NOTCH receptor expression within the DE itself, consistent with reported roles for intra-epithelial WNT signaling in maintaining stemness[54] and NOTCH signaling in cell fate specification[12]. Furthermore, our findings suggested the presence of other regulatory mechanisms, such as BMP signaling[55, 56], which we observed in the reparative zone (Supplementary Fig. 7e).

The mechanisms explored in this study may hold translational potential for regenerative dentistry. The translational potential of *DLX6-AS1*$^+$ cells resides in their capacity for lineage-specific differentiation. We employed a complementary validation strategy, using primitive, multipotent *DLX6-AS1*$^+$ DMSCs to test the instructive capacity of WNT-NOTCH signaling, and conversely, using the physiologically relevant *DLX6-AS1*$^+$ DPSCs to confirm the pathway's functional role in odontogenic differentiation. Through the recapitulation of developmental signals *in vitro* (WNT-NOTCH sequential stimulation), our studies demonstrated enhanced mineralization efficiency, establishing a framework for dental pulp-derived therapeutic interventions. The efficacy of *DLX6-AS1*$^+$ dental pulp stem cells in promoting dentin bridge formation in murine injury models underscored their therapeutic potential.

As we consider the path from these findings to potential clinical application, it is prudent to also address the complexities and assumptions inherent in our model. First, our reductionist approach, using sequentially delivered recombinant ligands, helped to isolate pathway-specific contributions but does not fully replicate the complex spatio-temporal gradients of a physiological niche. Second, while the soluble JAG1-Fc protein[57, 58] was sufficient to explore the biological principle[59, 60], its clinical translation faces challenges in localization and controlled release. The development of next-generation biologics, such as Artificially

Intelligent-designed soluble NOTCH agonists[61], may offer a path forward. Finally, future investigations should address the development of biomaterial scaffolds that simulate extracellular matrix signals and maintain signaling gradients *in situ*[62]. Additionally, subsequent studies must account for the biomechanical and biochemical complexities inherent to the dental pulp microenvironment. Furthermore, the intricate interplay between WNT-NOTCH and other signaling cascades warrants comprehensive investigation.

In conclusion, our study delineated the spatiotemporal dynamics of WNT-NOTCH signaling during human tooth development and identified *DLX6-AS1*$^+$ DP cells as potentially odontoblast progenitors. Through the integration of omics-driven discoveries with functional validation, our investigations established a developmental framework for utilizing DPSCs in regenerative dentistry. While challenges remain in translating these mechanistic insights into clinical applications, this work demonstrated the therapeutic potential of signaling pathway modulation and cell-based approaches in addressing the current limitations of dental tissue repair and regeneration.

### Limitations of the study

In this study, scRNA-seq and ST data from human tooth tissues at multiple time points were analyzed with a limited number of samples. Considering the complexity of odontoblast differentiation as a result of epithelial-mesenchymal interaction process, only significantly changed signaling pathways were considered when developing the regeneration strategy. In future studies, lineage tracing models could be developed for *DLX6-AS1*$^+$ DP cells, and *DLX6-AS1*$^+$ DPSCs might be isolated based on a membrane marker for cell sorting. Also, the functional difference between *DLX6-AS1*$^+$ and *NR2F1*$^+$*TWIST1*$^+$ DP cells needs to be further elucidated.

## METHODS

### Ethical approval and consent

This study was conducted under approval from the Ethics Commissions of Beijing Friendship Hospital (2021-P2-198-02), Beijing Laboratory of Oral Health (Z2022SY064), and Beijing Obstetrics and Gynecology Hospital (2023-KY-082-01), all affiliated with Capital Medical University (CMU). All research involving human biological materials was performed in accordance with the Declaration of Helsinki and the 2021 ISSCR Guidelines for Stem Cell Research and Clinical Translation. Written informed consent was obtained from all donors for the use of human embryonic tissues, and no financial compensation was provided. All animal experiments were performed in accordance with relevant guidelines and regulations and were approved by the Ethics Committee of Capital Medical University (AEEI-2023-087).

### Tissue collection

Human embryonic tissues were obtained from the Beijing Obstetrics and Gynecology Hospital following legally and ethically approved protocols. A total of eight embryos were analyzed. Specifically, scRNA-seq was performed on two replicates per stage across 7-8, 9-10, 12, and 15 PCW, while ST was performed on two replicates per stage across 9-10, 12, and 15 PCW. In all cases, each replicate (n=2 per stage) comprised one incisor and one molar from a distinct embryo. Due to the early developmental stage of the tissues, the sex of the embryos was not determined. All collected human embryonic tooth germ samples were entirely consumed during the single-cell and spatial transcriptomic experimental procedures and were therefore destroyed. Sample processing followed previously established protocols[9, 28]. In brief, incisor and molar tooth germs were dissected in DEPC-treated ice-cold phosphate buffered saline (PBS) (Gibco, 10010023; Invitrogen, AM9906). The isolated specimens were washed in cold PBS and processed for scRNA-seq. For ST analysis, dissected mandibles were immersed in pre-cooled isopentane (Sigma Aldrich, 4583) at -80°C and embedded in O.C.T. compounds (Sakura, 4583). Single-cell transcriptomic data for stages 17-24 PCW were obtained from Shi et al.[26] (available at: https://data.mendeley.com/datasets/v3wgx8pm5y/1). The sex of the embryos was not reported in the original study. Young pulp single-cell data were accessed from Gene Expression Omnibus (GEO) datasets. This included dataset GSE202476[27], derived from an immature third molar of a 13-year-old male donor, and dataset GSM4365609[25], from a tooth apical papilla with approximately two-thirds root completion where the donor's sex was not reported. ST data at 20 PCW were acquired from Shi et al[26]. Consistent with the SAGER guidelines, we report that sex was not considered as a biological variable in our study design because it was either not determined for early-stage embryonic samples or not reported in the integrated external datasets. Consequently, no sex-based analyses were performed, and data could not be disaggregated by sex.



**Cell culture**

Primary DE and mesenchymal cells were isolated from 12 PCW tooth germs. Tooth germs were enzymatically dissociated using 1.2 U/ml dispase II (Gibco, 17105041) and 20 U/ml DNase I (Gibco, 10104159001) for 10 minutes at room temperature. Epithelial and mesenchymal tissues were mechanically separated using fine needles. The DE tissues were dissociated and cultured in calcium chloride-free Keratinocyte Serum-free Medium (Gibco, A15170-01) supplemented with 15% FBS (Gibco, A5670401).

According to previous method[9, 63], DMSCs were enzymatically isolated using 3 mg/ml collagenase type I (Sigma-Aldrich, C0130) and 4 mg/ml dispase II for 1 hour at 37°C. Cells were maintained in α-MEM medium (Gibco, 12561072) supplemented with 15% FBS and antimicrobial agents (100 units/ml penicillin, 100 mg/ml streptomycin, 25 μg/ml Amphotericin B; Gibco, 15070063) at 37°C in 5% $CO_2$.

DPSCs were isolated following established protocols[64]. The pulp chamber was exposed after surface cleaning, and pulp tissue was enzymatically dissociated with collagenase at 37°C for 1 hour. Dissociated cells were filtered through a 70-μm mesh and cultured in supplemented α-MEM medium under standard conditions.

Human keratinocytes were obtained from Shanghai Jinyuan Biotechnology Co., Ltd (JY-J068) and cultured in Keratinocyte Serum-free Medium (Gibco, A15170-01) according to established protocols[65]. Cells were cultured for 36 hours prior to tissue recombination experiments.

**scRNA-seq**

**Data preprocessing and integration.** ScRNA-seq was performed at CapitalBio Technology (Beijing) using the Single Cell 3' GEM, Library & Gel Bead Kit V3.1 and Chromium Single Cell B Chip Kit. Cell suspensions were loaded onto a Chromium controller for single-cell gel bead generation. Each channel was loaded with approximately 6,000 cells, yielding ~3,000 target cells for amplification. Library quality was assessed using an Agilent 2400 bioanalyzer. Libraries were constructed according to manufacturer's protocols and sequenced on an Illumina Novaseq 6000 platform with paired-end 150 bp reads, targeting $\geqslant$100,000 reads per cell. Illumina NovaSeq 6000 software (v1.7) was used for sequencing data collection.

To ensure robust and unbiased comparison, all datasets underwent a standardized pre-processing and integration workflow using the Seurat R package (v4.4.0). For each dataset independently, the raw gene expression matrix was used to create a Seurat object. Low-quality cells were filtered out based on the following criteria: cells with fewer than 200 detected genes, more than 2500 detected genes, or a mitochondrial gene content exceeding 5% were removed. Following quality control, data was normalized using the NormalizeData function with a "LogNormalize" method and a scale factor of 10,000. The top 2000 most highly variable genes (HVGs) were identified for each dataset using the FindVariableFeatures function.

For integration, the pre-processed Seurat objects were merged. The merged data was then scaled using the ScaleData function. To correct for technical batch effects arising from different sequencing platforms, sample preparations, and laboratories, we utilized the Harmony algorithm (v0.1.1)[66]. Principal Component Analysis (PCA) was performed on the scaled data, and the RunHarmony function was executed on the resulting PCA embeddings, using the dataset of origin (orig.ident) as the batch variable.

**Dimensionality reduction, clustering, and cell type annotation.** All subsequent downstream analyses were performed on the Harmony-corrected embeddings. Uniform Manifold Approximation and Projection (UMAP) was run on the top 30 Harmony dimensions for 2D visualization. Cell clustering was performed by first running FindNeighbors on the same Harmony dimensions, followed by FindClusters with a resolution of 0.4. Cluster-specific markers were identified using the FindMarkers function (Wilcoxon rank-sum test).

Cell type annotation was manually curated based on the expression of known canonical markers, tooth-specific genes, and published reference data. The quality of data integration was visually validated by coloring the UMAP by developmental stage to confirm proper mixing of cells, and by generating VlnPlots and FeaturePlots for key markers to verify consistent expression patterns across original batches.

**Differential expression and functional enrichment analysis.** Differentially expressed genes (DEGs) between clusters were identified using the FindMarkers function on the original, uncorrected normalized counts. DEG selection criteria included a Bonferroni-adjusted *P*-value < 0.05 and an average $\log_2$(Fold Change) > 0.25. Functional annotation of significant genes was performed using the clusterProfiler package (v4.2.2) for Gene Ontology (GO) and Kyoto Encyclopedia of Genes and Genomes (KEGG) pathway analyses. To analyze specific populations, DE and DP cells were subset using the WhichCells function. Following the identification of pathway-specific ligands and receptors, gene expression data were retrieved using Seurat's FetchData function. Expression patterns were visualized through dot plots, pie charts, violin plots, and Sankey diagrams using Seurat's DotPlot, VlnPlot, and R's ggplot functions. To quantify the relative contribution of signaling pathways, we selected only the ligand and receptor genes that were stably detected in our single-cell data for the DE or DPL. Genes not detected in either population were excluded from the calculation and display. For a given gene set, we first extracted the normalized expression values for each gene in all individual cells within the DE and DPL. We then calculated a total expression score for each population by summing the expression values of all genes in the set across all cells of that population. Finally, the proportions shown in the pie charts were calculated.

**Developmental trajectory analysis.** Cell developmental trajectories were analyzed using VECTOR methodology as described by Zhang et al.[34]. Code is available at: https://github.com/jumphone/Vector. The analysis pipeline comprised: (1) dimensionality reduction through principal component analysis (PCA), with component selection based on explained variance; (2) identification of starting cells (SCs) using quantile polarization (QP) scores; (3) data visualization via UMAP; and (4) inference of RNA dynamics directions based on UMAP positioning and network distances from SCs. The UMAP space was segmented into pixels, and developmental trajectories were reconstructed by integrating positional information, QP scores, and inter-pixel distances.

**Branching trajectory analysis.** Branching trajectory analysis of DP cells was performed using Monocle 2 software (v2.18.0). Branch-specific gene expression programs were identified through Branched Expression Analysis Modeling (BEAM). This approach enabled the detection of genes with branch-dependent regulation patterns along the DP cell developmental trajectory.

## ST analysis

**ST data generation.** ST analysis was conducted at CapitalBio Technology (Beijing). Tissue cryosections (10- μ m) were mounted on GEX arrays and processed through sequential steps: incubation at 37℃, fixation at -20℃, and H&E staining. Sample wells were prepared using a Slide Cassette. Permeabilization was performed with 70 μL enzyme solution, followed by SSC washing and reverse transcription. After first-strand synthesis, samples underwent KOH treatment and second-strand synthesis. cDNA amplification was performed on a S1000TM Touch Thermal Cycler. Visium spatial libraries were prepared according to standard protocols and sequenced on an Illumina NovaSeq6000 with paired-end 150 bp reads, targeting ⩾100,000 reads per spot. Illumina NovaSeq 6000 software (v1.7) was used for sequencing data collection.

**Integration of scRNA-seq and ST data.** To overcome the multi-cellular resolution and accurately map cell populations in a spatial context, we implemented an integrative analysis strategy combining our high-resolution scRNA-seq data with the spatial transcriptomics data[9, 67]. Using the FindTransferAnchors and TransferData functions within the Seurat toolkit, we projected the cell type annotations derived from our scRNA-seq atlas (the 'reference') onto each spatial spot of the ST data (the 'query'). This process calculates a prediction score for each cell type at every spot, effectively deconvoluting the mixed cellular transcriptomes. The dominant cell type with the highest score was then used to assign an identity to each spot, enabling the visualization of cell population distributions. Gene expression patterns were visualized using the SpatialFeaturePlot function.

## RNA scope *in situ* hybridization

RNAscope Multiplex Fluorescent Assay (Advanced Cell Diagnostics, 320850) was performed on 5-μm cryosections of tissues fixed overnight in 4% paraformaldehyde at room temperature. Sections underwent target retrieval at 95-100°C for 5 minutes, followed by protease treatment (Advanced Cell Diagnostics, 310-100) at 40°C for 7 minutes. *DLX6-AS1* probe (Advanced Cell Diagnostics, 569491-C2) hybridization was conducted at 40°C for 2 hours. Signal amplification was performed using RNAscope Multiplex Fluorescent Reagent Kit, with detection via TSA Plus Cyanine 3 (PerkinElmer, NEL751A). Nuclei were counterstained with 4',6 - diamidino - 2 - phenylindole (DAPI). Nikon NIS-Elements (v5.4) was used for image acquisition.

## *DLX6-AS1*$^+$ DMSCs and *DLX6-AS1*$^+$ DPSCs

A lentiviral vector was constructed by replacing the CMV promoter in GV814 vector (CMV-EGFP-MCS-SV40-Puromycin) with the *DLX6-AS1* promoter sequence (NR_015448-promoter, positions 4836-6835). The construction and packaging of the resultant lentiviral vector (NR_015448-promoter-EGFP-SV40-

Puromycin) were performed by GeneChem. The full nucleotide sequence of the constructed vector and the inserted promoter region are provided in Supplementary Data 2. The viral particles were produced by co-transfecting the lentiviral construct with packaging plasmids into 293T cells. The target cells were infected with the lentivirus, and the cells positive for the reporter gene were screened to identify the cell population with an active promoter of the target gene. Under endogenous conditions, when the promoter is active in cells, it drives the expression of the reporter gene. As a corresponding control, the empty vector pLenti-Ubi-MCS-EGFP-IRES-Puromycin was used. DMSCs or DPSCs were seeded at $1\times10^5$ cells/well in 12-well plates and infected at 30% confluence using an MOI of 50. After 16 hours, medium was replaced and cells were cultured for 72 hours. Stable transformants were selected using puromycin (1 μg/ml, Sigma Aldrich, P8833) for 6 days, with medium changes every 2 days. Infection efficiency was confirmed by fluorescence microscopy.

**WNT-NOTCH sequential stimulation**

*DLX6-AS1*$^+$ cells were cultured in the α-MEM medium (Gibco, 12561072) supplemented with either WNT proteins (WNT6, OriGene, TP762653; WNT7B, CUSABIO, CSB-EP026142HU; WNT10B, CUSABIO, CSB-EP026130HU; all at 10 ng/ml) or JAG1 (10 ng/ml, MCE, HY-P70399). Sequential stimulation consisted of 7 days WNT treatment followed by 7 days JAG1 treatment, with medium changes every 2 days.

**Co-culture system**

To ensure the robustness of our knockdown experiments, we initially designed three distinct siRNA sequences for each target gene (*WLS* and *JAG1*). We then tested all three in vitro to screen for the one that demonstrated the highest knockdown efficiency (Supplementary Fig. 5g). DE cells were transfected with 40 nmol/L *WLS* or *JAG1* siRNAs (Sangon Biotech) using Lipofectamine RNAiMAX (Invitrogen, 13778030) in Opti-MEM (Invitrogen, 31985070). After 12 hours, medium was replaced with α-MEM (Gibco, 12561072). *DLX6-AS1*$^+$ DMSCs ($2.5\times10^4$ cells/well) were seeded in transwell upper chambers and co-cultured with transfected epithelial cells for 7 days. The 'pre+ and post+' condition specifically involved a transfer of the upper chamber: Days 0-3.5 ('pre+' phase): The transwell upper chambers containing *DLX6-AS1*$^+$ DMSCs were first co-cultured for 3.5 days with the DE cells that had been pre-treated with siRNA-*WLS.* Days 3.5-7 ('post+' phase): Subsequently, these same upper chambers were physically transferred to new wells containing DE cells that had been pre-treated with siRNA-*JAG1* and were co-cultured for the remaining 3.5 days.

All siRNA oligonucleotides were chemically synthesized and purified by Sangon Biotech. The sequences were as follows:

si-*WLS*-1: 5'-UCAUGUUUUCUAUAAUUGCCC-3'

si-*WLS*-2: 5'-ACAUUUCACCGACAUGUAGGA-3'
si-*WLS*-3: 5'-ACCAUUUUGUCUUGUGAUGGU-3'
si-*JAG1*-1: 5'-UUGAACAAGCUCACAUACCUG-3'
si-*JAG1*-2: 5'-UAAUUGAUAACUUUCCAGCUG-3'
si-*JAG1*-3: 5'-UAAAGUCGUAGUUAACACCAG-3'
siRNA-NC: 5'-ACGUGACACGUUCGGAGAA-3'

**Western blot**

Protein samples were separated on Mini-PROTEAN TGX Gels (Bio-Rad, 4561093) and transferred to membranes using the Trans-Blot Turbo system (Bio-Rad, 1704156). After blocking, membranes were probed with primary antibodies against DSPP (1:1,000, Proteintech, 55396-1-AP), LEF1 (1:1,000, Proteintech, 14972-1-AP), HEY1 (1:1,000, Proteintech, 19929-1-AP), and GAPDH (Proteintech, 60004-1-Ig, Clone 1E6D9). Following HRP-conjugated secondary antibody incubation, signals were detected using the ChemiDoc MP Imaging System (Bio-Rad Image Lab software v6.1). Unprocessed scans of all blots are provided in the Source Data file.

**Alkaline phosphatase (ALP) staining and Alizarin red S staining**

For ALP activity assessment, cells were fixed in 4% paraformaldehyde after 14 days of induction and stained using an ALP Assay Kit (Sigma Aldrich, MAK530). Mineralization was evaluated after 21 days of induction using 2% Alizarin red S solution (Sigma Aldrich, A5533). Leica Application Suite X (LAS X) software (v3.7) was used for brightfield image acquisition. For quantification, stained minerals were dissolved in 10% cetylpyridinium chloride (Sigma Aldrich, C5911) and measured spectrophotometrically at 562 nm.

**IF staining**

Samples were processed through sequential steps of trypsin treatment, permeabilization (0.5% PBST), hydrogen peroxide treatment, and goat serum blocking. Primary antibodies were used at a dilution of 1:200. Primary antibodies were applied against: DSPP (Abcam, ab216892), Ki67 (Cell Signaling Technology, 9129, Clone D3B5), KRT14 (Abcam, ab119695, Clone LL002), WNT6 (Abcam, ab50030), WNT7B (Proteintech, 10605-1-AP), WNT10B (Abcam, ab70816), LRP6 (Santa Cruz, sc-25317, Clone C-10), JAG1 (Abcam, ab300561, Clone EPR26388-51), NOTCH2 (Abcam, ab313453, Clone EPR28701-38), DKK1 (Abcam, ab61034, Clone EPR4759), SFRP1 (Proteintech, 26460-1-AP), HEY1 (Proteintech, 19929-1-AP), LEF1 (Abcam, ab137872, Clone EPR2029Y), BMP2 (Abcam,ab214821), BMP4 (Abcam, ab39973), GFP(CST, 2956, Clone D5.1) and rabbit IgG isotype control (CST, 3900, Clone DA1E) were added. Sections were

subsequently incubated with appropriate secondary antibodies and counterstained with DAPI. Regions of interest (ROIs) were delineated based on tissue architecture visualized by DAPI staining. For Supplementary Fig. 3g, the Mean Fluorescence Intensity (MFI) of WNT6, WNT7B, WNT10B, and JAG1 was measured within the DE, while the MFI of LRP6, NOTCH2, DKK1, SFRP1, HEY1, and LEF1 was measured within the DPL. Data are presented as mean ± SEM. Nikon NIS-Elements (v5.4) was used for image acquisition.

**qRT-PCR analysis**

RNA was isolated using the RNeasy Kit (Qiagen, 74104) and reverse transcribed using the Transcriptor First Strand cDNA Synthesis Kit (Roche, 04379012001). Quantitative PCR was performed using SsoAdvanced Universal SYBR Green Supermix (Bio-Rad, 172-5270). Bio-Rad CFX Maestro software (v2.0) was used for data collection.

The primers used for RT-qPCR were synthesized by Sangon Biotech and as follows:

*GAPDH*:

Forward: 5'-GCACCGTCAAGGCTGAGAAC-3'

Reverse: 5'-ATGGTGGTGAAGACGCCAGT-3'

*DMP1*:

Forward: 5'-GCAGAGTGATGACCCAGAG-3'

Reverse: 5'-GCTCGCTTCTGTCATCTTCC-3'

*DSPP*:

Forward: 5'-GGGATGTTGGCGATGCA-3'

Reverse: 5'-CCAGCTACTTGAGGTCCATCTTC-3'

*DLX6-AS1*:

Forward: 5'-AGTTTCTCTCTAGATTGCCTT-3'

Reverse: 5'-ATTGACATGTTAGTGCCCTT-3'

*MEPE*:

Forward: 5'-GGCCAGTGACTGCGATTAAAC-3'

Forward: 5'-CCTTCGAGTGTGCTTTAGCAT-3'

*ALP*:

Forward: 5'-AACATCAGGGACATTGACGTG-3'

Reverse: 5'-GTATCTCGGTTTGAAGCTCTTCC-3'

**Animals**

Male BALB/c nude mice (*Mus musculus*), 8 weeks of age, were obtained from Charles River Laboratories. These mice possess a BALB/c genetic background carrying the *Foxn1$^{nu}$* mutation The mice were housed in a specific pathogen-free facility at Capital Medical University under controlled environmental conditions. Specifically, housing conditions included a 12-hour light/12-hour dark cycle, a constant ambient temperature of 22 ± 2°C, and a relative humidity of 55 ± 10%. The animals were housed in individually ventilated cages with free access to standard sterilized rodent chow and water. For all *in vivo* experiments, mice were randomly assigned to experimental groups (n = 5 mice per group). Only male mice were used in this study to avoid potential confounding effects from hormonal fluctuations associated with the female estrous cycle, which could influence tissue regeneration and inflammatory responses.

**Recombination and subrenal culture**

Human keratinocyte cells and mesenchymal cells (DMSCs, *DLX6-AS1*$^{+}$ DMSCs, or WNTs-pretreated *DLX6-AS1*$^{+}$ DMSCs) were pelleted separately at 150x g for 5 minutes. Cell pellets (1×10$^{5}$ cells/0.25 μL each) were sequentially injected into Cellmatrix Type I-A (5 μL, Nitta Gelatin Inc, 631-00651) and incubated at 37°C for 30 minutes for gelation[68]. Recombinants were cultured in supplemented DMEM (20% FBS, 100 U/mL penicillin/streptomycin, 0.18 mg/mL L-ascorbic acid) for 3 days before transplantation under the kidney capsule of adult male nude mice. WNTs or JAG1-loaded PLGA (75:25) (MCE, HY-B2247A) was co-transplanted. For the control group, PLGA microspheres loaded with Bovine Serum Albumin (BSA) were used[69]. Recombinants were harvested after 3 months for histological analysis.

**H&E staining and Masson's trichrome staining**

Paraffin-embedded samples were processed for H&E staining (Servicebio, G1076) and Masson's trichrome staining (Servicebio, G1006) following manufacturers' protocols.

**Tooth damage model**

Under anesthesia, cavities were created in the maxillary first molars of adult male nude mice until pulp visibility. Pulp exposure was achieved using a 27G 3/4 gauge needle[70]. After pulp exposure, different treatment interventions were applied according to experimental groups, with one group receiving WNTs-pretreated *DLX6-AS1*$^{+}$ DPSCs combined with JAG1 injection at the exposure site. Cavities were sealed with glass ionomer cement (3M ESPE, 56906). Samples were collected 21 days post-operation.

**MicroCT analysis**

Samples were scanned using a high-resolution micro-computed tomography (μCT) system (SkyScan 1276, Bruker, Kontich, Belgium) located at the Core Facility Center, Capital Medical University. The scans were

performed with an isotropic voxel size of 7 μm. Two- and three-dimensional reconstructions were generated for dental defect analysis.

### Scanning Electron Microscopy (SEM) Analysis

Mouse tooth samples were fixed in 2.5% glutaraldehyde. Dried samples were mounted on aluminum stubs, sputter-coated with a 15 nm gold-palladium layer and imaged using a scanning electron microscope. image were acquired using a Thermo Scientific Apreo 2C SEM controlled by Thermo Scientific microscope control software.

### Combined detection by RNAscope® multiplex fluorescent assay and IF

A combined RNAscope® and immunofluorescence (IF) protocol was performed following the manufacturer's guidelines for the RNAscope® Multiplex Fluorescent v2 Assay kit (Advanced Cell Diagnostics, 323100). Briefly, after tissue preparation and target retrieval, the IF portion of the protocol was initiated. Sections were blocked and then incubated with primary antibodies overnight. Following primary antibody incubation, sections were treated with Protease Plus. The RNAscope® portion was then continued with probe hybridization, signal amplification, and signal development using the TSA detection system (PerkinElmer, NEL751A). Finally, nuclei were counterstained with DAPI.

### Statistical analysis

ImageJ (v1.53) was used for quantification and processing of confocal, widefield, and SEM images. GraphPad Prism (v9.0) was used for statistical analysis and graphing. Results were expressed as mean ± SEM. Statistical significance for two-group comparisons was determined by a two-sided unpaired Student’s t-test. For multiple-group comparisons, a one-way ANOVA followed by Tukey’s multiple comparisons test was used. A P-value < 0.05 was considered statistically significant.

## DATA AVAILABILITY

The single-cell RNA sequencing and spatial transcriptomics data for developmental stages 7-8, 9-10, 12, and 15 PCW have been deposited in the Genome Sequence Archive (Genomics, Proteomics & Bioinformatics 2025) in the National Genomics Data Center (Nucleic Acids Res 2025), China National Center for Bioinformation / Beijing Institute of Genomics, Chinese Academy of Sciences, under accession number HRA013557 [https://ngdc.cncb.ac.cn/gsa-human/browse/HRA013557]. The single-cell and spatial transcriptomics data of human embryonic tooth development (stages 17-24 PCW) are available in the Mendeley Data repository under DOI: 10.17632/v3wgx8pm5y.1[26] (https://data.mendeley.com/datasets/v3wgx8pm5y/1). The young dental pulp single-cell data are available

in the Gene Expression Omnibus (GEO) database under accession numbers GSE202476 [https://www.ncbi.nlm.nih.gov/geo/query/acc.cgi?acc=GSE202476] and GSM4365609 [https://www.ncbi.nlm.nih.gov/geo/query/acc.cgi?acc=GSM4365609]. Source data are provided with this paper.

## CODE AVAILABILITY

The code in this study is available on GitHub at https://github.com/weiwei2012/NCOMMS-2538526, and the pipelines are detailed in the Methods.

## REFERENCES


1. Marshall GW, Jr., Marshall SJ, Kinney JH, Balooch M. The dentin substrate: structure and properties related to bonding. *J Dent* **25**, 441-458 (1997).
2. Wang HS, Yang FH, Wang YJ, Pei F, Chen Z, Zhang L. Odontoblastic Exosomes Attenuate Apoptosis in Neighboring Cells. *J Dent Res* **98**, 1271-1278 (2019).
3. Smith AJ, Duncan HF, Diogenes A, Simon S, Cooper PR. Exploiting the Bioactive Properties of the Dentin-Pulp Complex in Regenerative Endodontics. *J Endod* **42**, 47-56 (2016).
4. Barron MJ, McDonnell ST, Mackie I, Dixon MJ. Hereditary dentine disorders: dentinogenesis imperfecta and dentine dysplasia. *Orphanet J Rare Dis* **3**, 31 (2008).
5. Kratochvilova L*, et al.* Ectodermal dysplasia: important role of complex dental care in its interdisciplinary management. *Eur J Paediatr Dent* **23**, 140-146 (2022).
6. Balic A, Thesleff I. Tissue Interactions Regulating Tooth Development and Renewal. *Curr Top Dev Biol* **115**, 157-186 (2015).
7. Caton J, Tucker AS. Current knowledge of tooth development: patterning and mineralization of the murine dentition. *J Anat* **214**, 502-515 (2009).
8. Yu T, Klein OD. Molecular and cellular mechanisms of tooth development, homeostasis and repair. *Development* **147**, (2020).
9. Zhang R*, et al.* Integrated multi-omics profiling characterizes the crucial role of human dental epithelium during tooth development. *Cell Rep* **44**, 115437 (2025).
10. Lee JM, Qin C, Chai OH, Lan Y, Jiang R, Kwon HE. MSX1 Drives Tooth Morphogenesis Through Controlling Wnt Signaling Activity. *J Dent Res* **101**, 832-839 (2022).
11. Kim R*, et al.* Early perturbation of Wnt signaling reveals patterning and invagination-evagination control points in molar tooth development. *Development* **148**, (2021).
12. Mitsiadis TA, Pagella P, Capellini TD, Smith MM. The Notch-mediated circuitry in the evolution and generation of new cell lineages: the tooth model. *Cell Mol Life Sci* **80**, 182 (2023).
13. Vainio S, Karavanova I, Jowett A, Thesleff I. Identification of BMP-4 as a signal mediating secondary induction between epithelial and mesenchymal tissues during early tooth development. *Cell* **75**, 45-58 (1993).
14. Yuan G*, et al.* The non-canonical BMP and Wnt/beta-catenin signaling pathways orchestrate early

tooth development. *Development* **142**, 128-139 (2015).
15. Zhang H, Gong X, Xu X, Wang X, Sun Y. Tooth number abnormality: from bench to bedside. *Int J Oral Sci* **15**, 5 (2023).
16. Li L, Tang Q, Kwon HE, Wu Z, Kim EJ, Jung HS. An Explanation for How FGFs Predict Species-Specific Tooth Cusp Patterns. *J Dent Res* **97**, 828-834 (2018).
17. Lin C*, et al.* FGF8-mediated signaling regulates tooth developmental pace during odontogenesis. *J Genet Genomics* **49**, 40-53 (2022).
18. Zhang R, Yang G, Wu X, Xie J, Yang X, Li T. Disruption of Wnt/beta-catenin signaling in odontoblasts and cementoblasts arrests tooth root development in postnatal mouse teeth. *Int J Biol Sci* **9**, 228-236 (2013).
19. Zhang R*, et al.* Odontoblast beta-catenin signaling regulates fenestration of mouse Hertwig's epithelial root sheath. *Sci China Life Sci* **58**, 876-881 (2015).
20. Liang Z*, et al.* Understanding the multi-functionality and tissue-specificity of decellularized dental pulp matrix hydrogels for endodontic regeneration. *Acta Biomater* **181**, 202-221 (2024).
21. Gozlan O, Sprinzak D. Notch signaling in development and homeostasis. *Development* **150**, (2023).
22. Sun K*, et al.* A Wnt10a-Notch signaling axis controls Hertwig's epithelial root sheath cell behaviors during root furcation patterning. *Int J Oral Sci* **16**, 25 (2024).
23. Bejoy J, Bijonowski B, Marzano M, Jeske R, Ma T, Li Y. Wnt-Notch Signaling Interactions During Neural and Astroglial Patterning of Human Stem Cells. *Tissue Eng Part A* **26**, 419-431 (2020).
24. Garcia-Alonso L*, et al.* Mapping the temporal and spatial dynamics of the human endometrium in vivo and in vitro. *Nat Genet* **53**, 1698-1711 (2021).
25. Krivanek J*, et al.* Dental cell type atlas reveals stem and differentiated cell types in mouse and human teeth. *Nat Commun* **11**, 4816 (2020).
26. Shi Y*, et al.* Spatiotemporal cell landscape of human embryonic tooth development. *Cell Prolif* **57**, e13653 (2024).
27. Ren H, Wen Q, Zhao Q, Wang N, Zhao Y. Atlas of human dental pulp cells at multiple spatial and temporal levels based on single-cell sequencing analysis. *Front Physiol* **13**, 993478 (2022).
28. Shen Z*, et al.* An atlas of early human mandibular endochondral and osteogenic paracrine signaling regions of Meckel's cartilage. *Proc Natl Acad Sci U S A* **122**, e2420466122 (2025).
29. Alghadeer A*, et al.* Single-cell census of human tooth development enables generation of human enamel. *Dev Cell* **58**, 2163-2180 e2169 (2023).
30. MacDonald BT, Tamai K, He X. Wnt/beta-catenin signaling: components, mechanisms, and diseases. *Dev Cell* **17**, 9-26 (2009).
31. Holzem M, Boutros M, Holstein TW. The origin and evolution of Wnt signalling. *Nat Rev Genet* **25**, 500-512 (2024).
32. Behrens J*, et al.* Functional interaction of beta-catenin with the transcription factor LEF-1. *Nature* **382**, 638-642 (1996).
33. Niessen K, Karsan A. Notch signaling in cardiac development. *Circ Res* **102**, 1169-1181 (2008).
34. Zhang F, Li X, Tian W. Unsupervised Inference of Developmental Directions for Single Cells Using

VECTOR. *Cell Rep* **32**, 108069 (2020).

35. Jing J*, et al.* Spatiotemporal single-cell regulatory atlas reveals neural crest lineage diversification and cellular function during tooth morphogenesis. *Nat Commun* **13**, 4803 (2022).
36. Bei M, Maas R. FGFs and BMP4 induce both Msx1-independent and Msx1-dependent signaling pathways in early tooth development. *Development* **125**, 4325-4333 (1998).
37. Chen S*, et al.* Runx2, osx, and dspp in tooth development. *J Dent Res* **88**, 904-909 (2009).
38. Gu X*, et al.* Profiling and functional characterization of long noncoding RNAs during human tooth development. *Int J Oral Sci* **17**, 38 (2025).
39. Liu L*, et al.* DLX6-AS1 regulates odonto/osteogenic differentiation in dental pulp cells under the control of BMP9 via the miR-128-3p/MAPK14 axis: A laboratory investigation. *Int Endod J* **57**, 1623-1638 (2024).
40. Liu Y, Graves DT, Wang S. Development and clinical application of human mesenchymal stem cell drugs. *Sci Bull (Beijing)* **68**, 860-863 (2023).
41. Liu Y*, et al.* Impact of allogeneic dental pulp stem cell injection on tissue regeneration in periodontitis: a multicenter randomized clinical trial. *Signal Transduct Target Ther* **10**, 239 (2025).
42. Huang GT, Gronthos S, Shi S. Mesenchymal stem cells derived from dental tissues vs. those from other sources: their biology and role in regenerative medicine. *J Dent Res* **88**, 792-806 (2009).
43. Lawson ND*, et al.* Notch signaling is required for arterial-venous differentiation during embryonic vascular development. *Development* **128**, 3675-3683 (2001).
44. Li J, Parada C, Chai Y. Cellular and molecular mechanisms of tooth root development. *Development* **144**, 374-384 (2017).
45. Wang Y*, et al.* Spatiotemporal dynamics of canonical Wnt signaling during embryonic eye development and posterior capsular opacification (PCO). *Exp Eye Res* **175**, 148-158 (2018).
46. Johnson MR*, et al.* A multifunctional Wnt regulator underlies the evolution of rodent stripe patterns. *Nat Ecol Evol* **7**, 2143-2159 (2023).
47. Lavicky J*, et al.* The Development of Dentin Microstructure Is Controlled by the Type of Adjacent Epithelium. *J Bone Miner Res* **37**, 323-339 (2022).
48. Xu Q*, et al.* Mechanoadaptive Responses in the Periodontium Are Coordinated by Wnt. *J Dent Res* **98**, 689-697 (2019).
49. Tamura M, Nemoto E. Role of the Wnt signaling molecules in the tooth. *Jpn Dent Sci Rev* **52**, 75-83 (2016).
50. Jarvinen E, Shimomura-Kuroki J, Balic A, Jussila M, Thesleff I. Mesenchymal Wnt/beta-catenin signaling limits tooth number. *Development* **145**, (2018).
51. Kalamakis G*, et al.* Quiescence Modulates Stem Cell Maintenance and Regenerative Capacity in the Aging Brain. *Cell* **176**, 1407-1419 e1414 (2019).
52. Dietrich B, Haider S, Meinhardt G, Pollheimer J, Knofler M. WNT and NOTCH signaling in human trophoblast development and differentiation. *Cell Mol Life Sci* **79**, 292 (2022).
53. Guo R*, et al.* Context-dependent regulation of Notch signaling in glial development and tumorigenesis. *Sci Adv* **9**, eadi2167 (2023).

54. Zhu X*, et al.* Intra-epithelial requirement of canonical Wnt signaling for tooth morphogenesis. *J Biol Chem* **288**, 12080-12089 (2013).
55. Fu H, Tan X, Ye L, Wang C. The glycoprotein Wnt6 regulates human dental papilla cells differentiation by canonical Wnt signaling pathway. *Arch Oral Biol* **141**, 105469 (2022).
56. Zhou T*, et al.* CDC42-mediated Wnt signaling facilitates odontogenic differentiation of DPCs during tooth root elongation. *Stem Cell Res Ther* **14**, 255 (2023).
57. Karanu FN*, et al.* The notch ligand jagged-1 represents a novel growth factor of human hematopoietic stem cells. *J Exp Med* **192**, 1365-1372 (2000).
58. Ba K*, et al.* Jagged-1-mediated activation of notch signalling induces adipogenesis of adipose-derived stem cells. *Cell Prolif* **45**, 538-544 (2012).
59. Roopenian DC, Akilesh S. FcRn: the neonatal Fc receptor comes of age. *Nat Rev Immunol* **7**, 715-725 (2007).
60. Vaccaro C, Zhou J, Ober RJ, Ward ES. Engineering the Fc region of immunoglobulin G to modulate in vivo antibody levels. *Nat Biotechnol* **23**, 1283-1288 (2005).
61. R M*, et al.* Design of soluble Notch agonists that drive T cell development and boost immunity. *Cell*, (2025).
62. Zhu M*, et al.* In vivo engineered extracellular matrix scaffolds with instructive niches for oriented tissue regeneration. *Nat Commun* **10**, 4620 (2019).
63. Yalvac ME*, et al.* Human tooth germ stem cells preserve neuro-protective effects after long-term cryo-preservation. *Curr Neurovasc Res* **7**, 49-58 (2010).
64. Cao Y*, et al.* Adenovirus-mediated transfer of hepatocyte growth factor gene to human dental pulp stem cells under good manufacturing practice improves their potential for periodontal regeneration in swine. *Stem Cell Res Ther* **6**, 249 (2015).
65. Wang B*, et al.* Induction of human keratinocytes into enamel-secreting ameloblasts. *Dev Biol* **344**, 795-799 (2010).
66. Korsunsky I*, et al.* Fast, sensitive and accurate integration of single-cell data with Harmony. *Nat Methods* **16**, 1289-1296 (2019).
67. Fawkner-Corbett D*, et al.* Spatiotemporal analysis of human intestinal development at single-cell resolution. *Cell* **184**, 810-826 e823 (2021).
68. Wang F*, et al.* The cell re-association-based whole-tooth regeneration strategies in large animal, Sus scrofa. *Cell Prolif* **51**, e12479 (2018).
69. Ma Y*, et al.* Ror2-mediated non-canonical Wnt signaling regulates Cdc42 and cell proliferation during tooth root development. *Development* **148**, (2021).
70. Babb R, Chandrasekaran D, Carvalho Moreno Neves V, Sharpe PT. Axin2-expressing cells differentiate into reparative odontoblasts via autocrine Wnt/beta-catenin signaling in response to tooth damage. *Sci Rep* **7**, 3102 (2017).


## ACKNOWLEDGEMENTS

We thank members of Beijing Laboratory of Oral Health for inspiring discussions. We sincerely thank Dr. Junjun Jing, Dr. Zhen Huang, and Dr. Min Liu for their valuable guidance. We also thank Dr. Chenjie Zhang and Dr. Rong Kang for their valuable help with the experiments. This work was supported by the National Key Research and Development Program (2022YFA1104401 to Zhipeng Fan); Beijing Municipal Government grant (Beijing Laboratory of Oral Health, PXM2021-014226-000041 to S.W.); Beijing Municipal Government (Beijing Scholar Program, PXM2021-014226-000020 to S.W.); National Natural Science Foundation of China (82030031 to S.W., 92149301 to S.W., 81991504 to Yi Liu, L2224038 to S.W., 82270945 to R.Z.); Innovation Research Team Project of Beijing Stomatological Hospital, Capital Medical University (CXTD202201 to S.W.); Chinese Research Unit of Tooth Development and Regeneration, Academy of Medical Sciences (2019-12M-5-031 to S.W.); Beijing Natural Science Foundation General Program (7252167 to R.Z.); Young Scientist Program of Beijing Stomatological Hospital, Capital Medical University (YSP202314 to W.W.).

## AUTHOR CONTRIBUTIONS STATEMENT

Conceptualization: S.W., R.Z., W.W., C.W.. Collected and analyzed scRNA-seq data: W.W., C.W., R.Z., Z.S.. Collected and analyzed image and ST data: W.W., C.W., R.Z., Z.S.. Methodology: W.W., C.W., J.S., M.H., X.G., H.Z., C.Z., J.W., Lei H., L.L., Y.Z., Lina H.. Funding acquisition: S.W., R.Z., W.W.. Writing – original draft: W.W., C.W.. Writing – review & editing: S.W., X.W., Z.S., R.Z., W.W., C.W..

## COMPETING INTERESTS STATEMENT

The authors declare no competing interests.

## SUPPLEMENTARY INFORMATION

Supplementary Fig. 1-7 and Supplementary Data 1-2.

## FIGURE LEGENDS

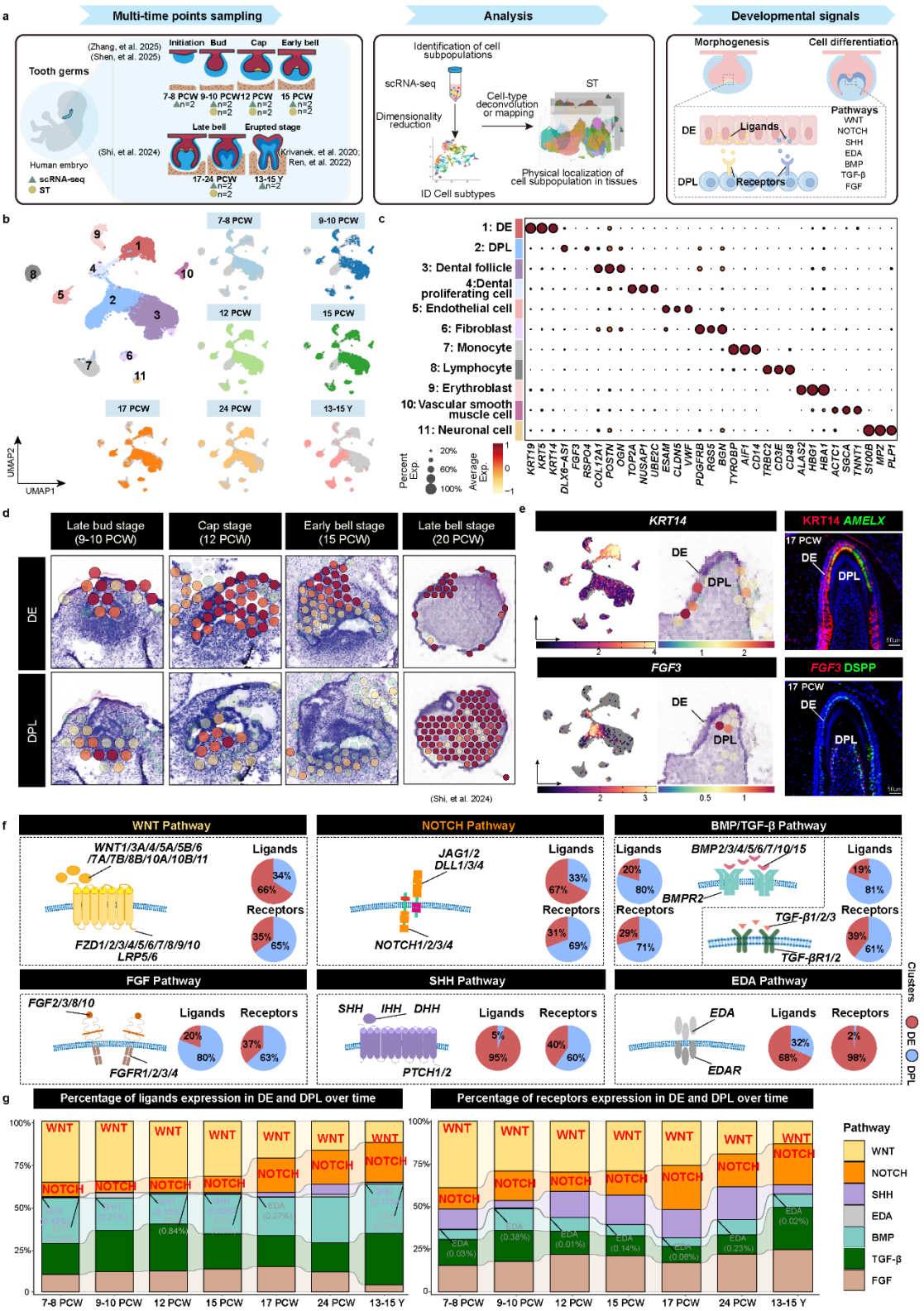


**Fig. 1. Single-cell and spatial transcriptomic insights into tooth developmental progression.**

(a) Experimental workflow schematic.

(b) UMAP (Uniform Manifold Approximation and Projection) of all cells from human tooth germs (n=2 biological replicates per stage; 7-8 post-conception weeks (PCW) to 13-15 years (Y)). Cells are colored by identity; smaller plots show stage-specific compositions.

(c) Dot plot of marker gene expression. Dot size indicates the percentage of cells expressing a gene; color reflects average expression level. Markers were identified using a two-sided Wilcoxon Rank Sum test with Bonferroni correction for multiple comparisons (adjusted $P < 0.05$, $\log_2$ fold change (FC) > 0.25, expressed in >25% of cells). DE, dental epithelium; DPL, DP lineage.

(d) Spatial deconvolution mapping scRNA-seq-defined cell types onto ST sections from late bud to late bell stages. Each colored circle represents a data-capturing spot, with its color indicating the predominant cell type inferred by integrating scRNA-seq data. Images are representative of n=2 biological replicates analyzed for each stage.

(e) UMAP and spatial plots for DE marker KRT14 and DPL marker FGF3. Validation on 17 PCW sections by RNAscope and immunofluorescence (IF). Top right: KRT14 (red, IF) co-localizes with AMELX (green, RNAscope). Bottom right: FGF3 (red, RNAscope) is adjacent to DSPP (green, RNAscope). Scale bars, 50 μm. Staining images are representative of three independent biological replicates with similar results.

(f) Relative proportions of developmental pathway ligands and receptors in DE and DPL, based on the total expression of each gene set within the respective populations. The pie charts of the BMP/TGF-β pathways depict information from two functionally distinct branches. Left: BMP pathway. Right: TGF-β pathway.

(g) Sankey diagram tracking the proportional expression of ligands (left) and receptors (right) for key pathways across development.

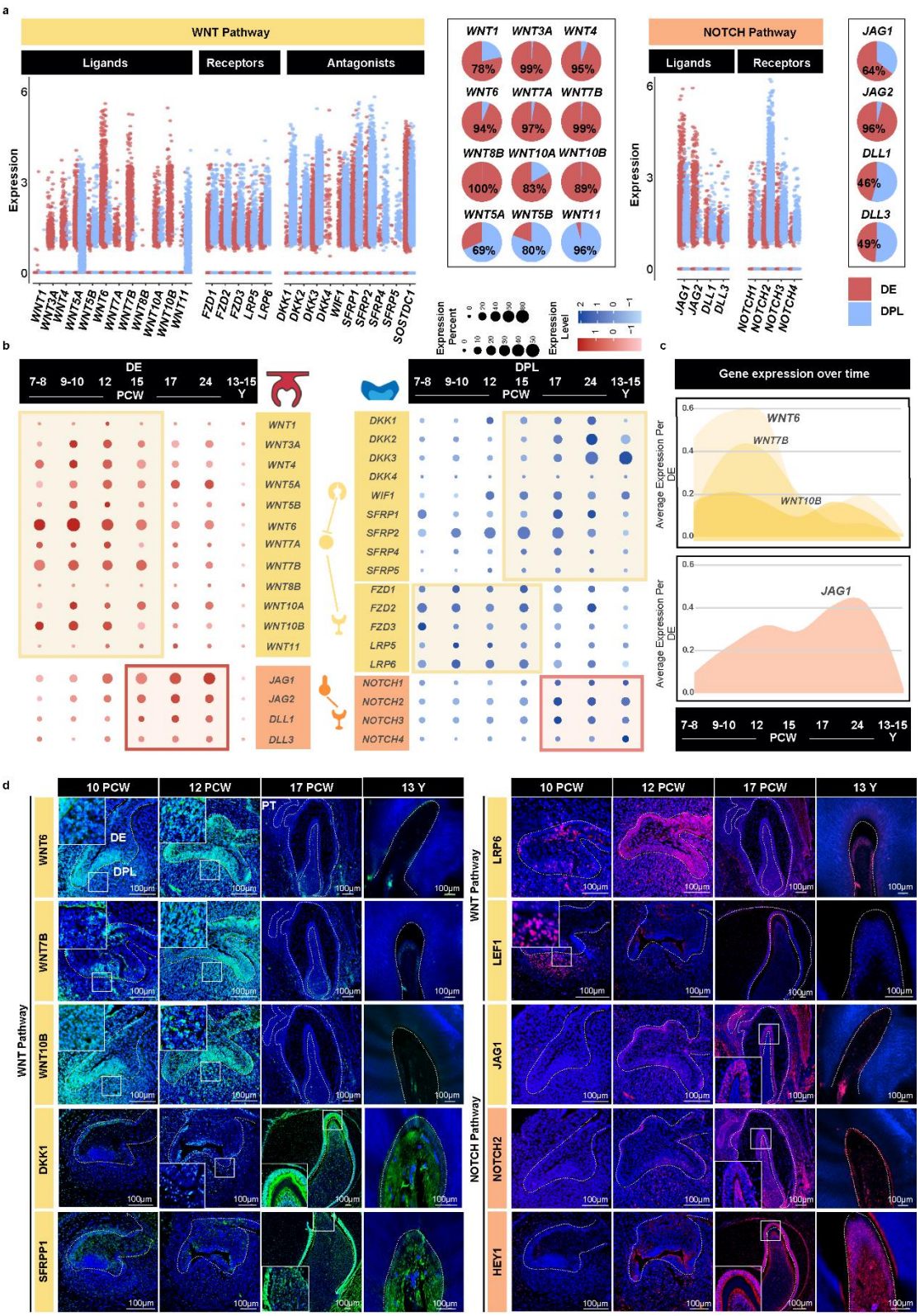


**Fig. 2. Spatiotemporal dynamics of WNT and NOTCH signaling during tooth development.**

(a) Split violin plots showing the expression distribution of WNT and NOTCH pathway components in DE (red) and DPL (blue). Each dot represents a single cell. Adjacent pie charts quantify the percentage of cells within the DE population expressing specific WNT and NOTCH ligands.

(b) Dot plots illustrating the dynamic expression of WNT and NOTCH pathway genes in DE (left panel, red color scale) and DPL (right panel, blue color scale) across developmental stages. Dot size is proportional to the percentage of cells expressing the gene, and color intensity reflects the average z-score normalized expression level. PCW, post-conception weeks; Y, years.

(c) Line graphs tracking the average expression of key WNT (*WNT6*, *WNT7B*, *WNT10B*) and NOTCH (*JAG1*) ligands within the DE population over time.

(d) IF validation of the spatial localization of key WNT and NOTCH pathway proteins across different developmental stages. Target proteins (WNT6, WNT7B, WNT10B, DKK1, SFRP1, LRP6, LEF1, JAG1, NOTCH2, HEY1) are shown in green or red, with nuclei counterstained with DAPI (blue). Dotted lines outline the epithelial-mesenchymal boundary. Insets show magnified views of the indicated regions. Images are representative of experiments that were independently repeated three times with similar results (n=3 biological replicates). PT, permanent tooth. Scale bars: 100 μm.

Data in (a-c) are derived from scRNA-seq analysis of n=2 biological replicates per developmental stage.

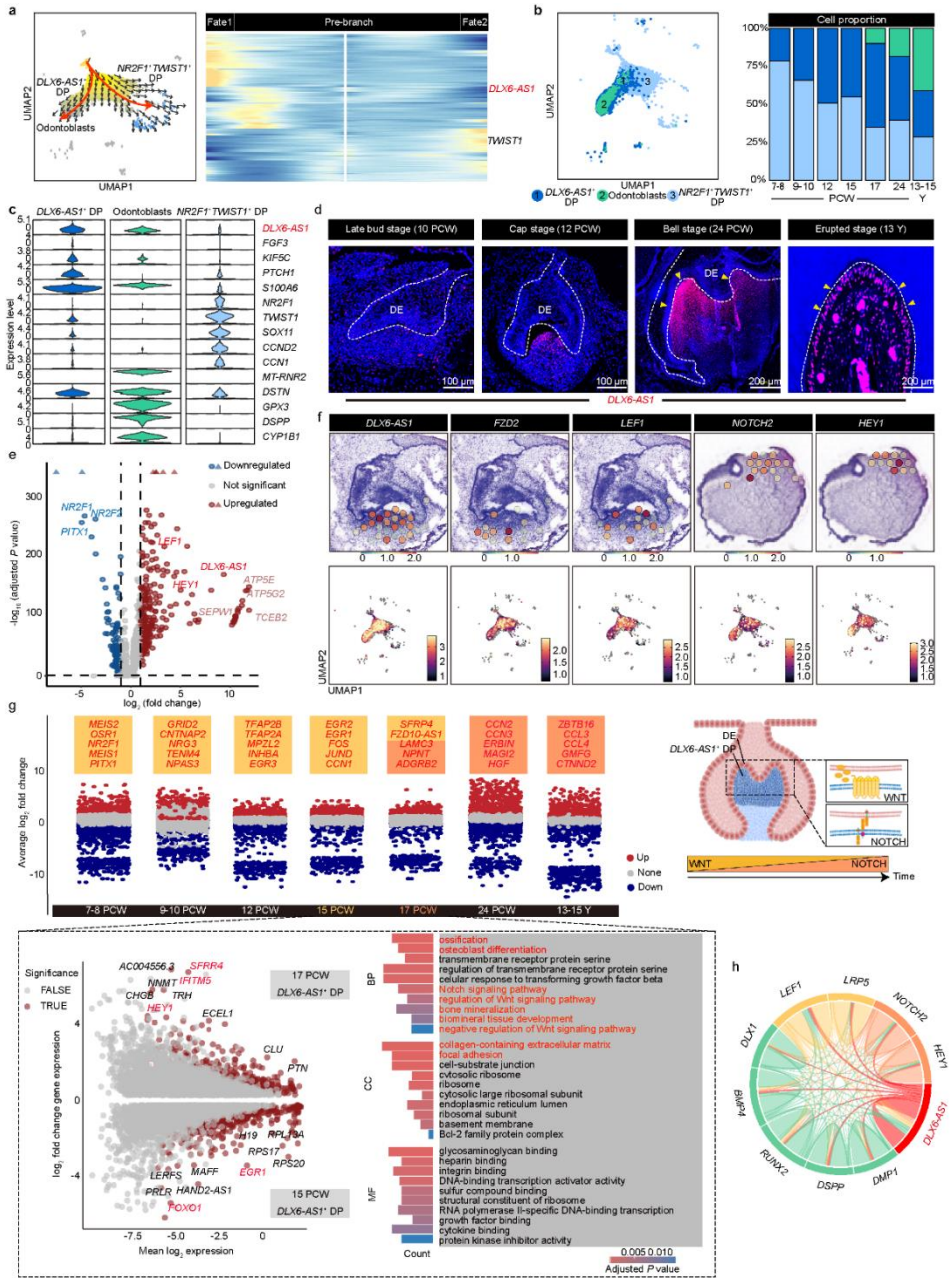

**Fig. 3. The domestication pattern of *DLX6-AS1*⁺ DP by epithelial WNT-NOTCH signaling pathway.**

(a) Vector field visualization (left) and heatmap of branch-dependent differentially expressed genes (DEGs) (right) along differentiation trajectories. Branch-dependent DEGs were identified using Branched Expression Analysis Modeling (q-value < 0.0001).

(b) UMAP visualization of DPL subpopulations (right) with temporal distribution of cell proportions (left)

(c) Expression distribution of genes across identified clusters.

(d) RNAscope staining of *DLX6-AS1* (red, arrowheads) in the human molar. Nuclei are DAPI-stained (blue), and dotted lines mark the epithelial-mesenchymal boundary. Images are representative of experiments

independently repeated three times with similar results (n=3 biological replicates). Scale bars: 100 μm for molars at 10 and 12 PCW; 200 μm for molars at 24 PCW and 13 Y.

(e) Volcano plot comparing *DLX6-AS1*$^+$ and *NR2F1*$^+$*TWIST1*$^+$ DP (red: *DLX6-AS1*$^+$ DP-enriched; blue: *NR2F1*$^+$*TWIST1*$^+$ DP-enriched; gray: non-significant). Dashed lines mark significance thresholds (adjusted $P < 0.05$, $|\log_2 FC| > 1.0$), determined by a two-sided Wilcoxon rank-sum test with Bonferroni correction. Genes with adjusted p-values of zero are shown as upward-pointing arrows at the top of the y-axis to indicate that their significance exceeds the plotted range.

(f) Spatial distribution (top) and UMAP FeaturePlots (bottom) of *DLX6-AS1*, *FZD2*, *LEF1*, *NOTCH2*, and *HEY1*.

(g) Temporal transcriptional dynamics in *DLX6-AS1*$^+$ DP. Top: Dot plot of stage-specific DEGs (two-sided Wilcoxon rank-sum test, Bonferroni correction). Bottom left: MA plot of DEGs between 17 and 15 PCW (two-sided Wilcoxon rank-sum test, Bonferroni correction). Bottom right: GO enrichment analysis (one-sided hypergeometric test, Benjamini-Hochberg correction).

(h) Chord diagram showing Pearson correlations among *DLX6-AS1*, WNT/NOTCH pathway components, and odontogenic factors.

Data in (a-c, e-h) are based on scRNA-seq and ST analyses from n=2 biological replicates per developmental stage.

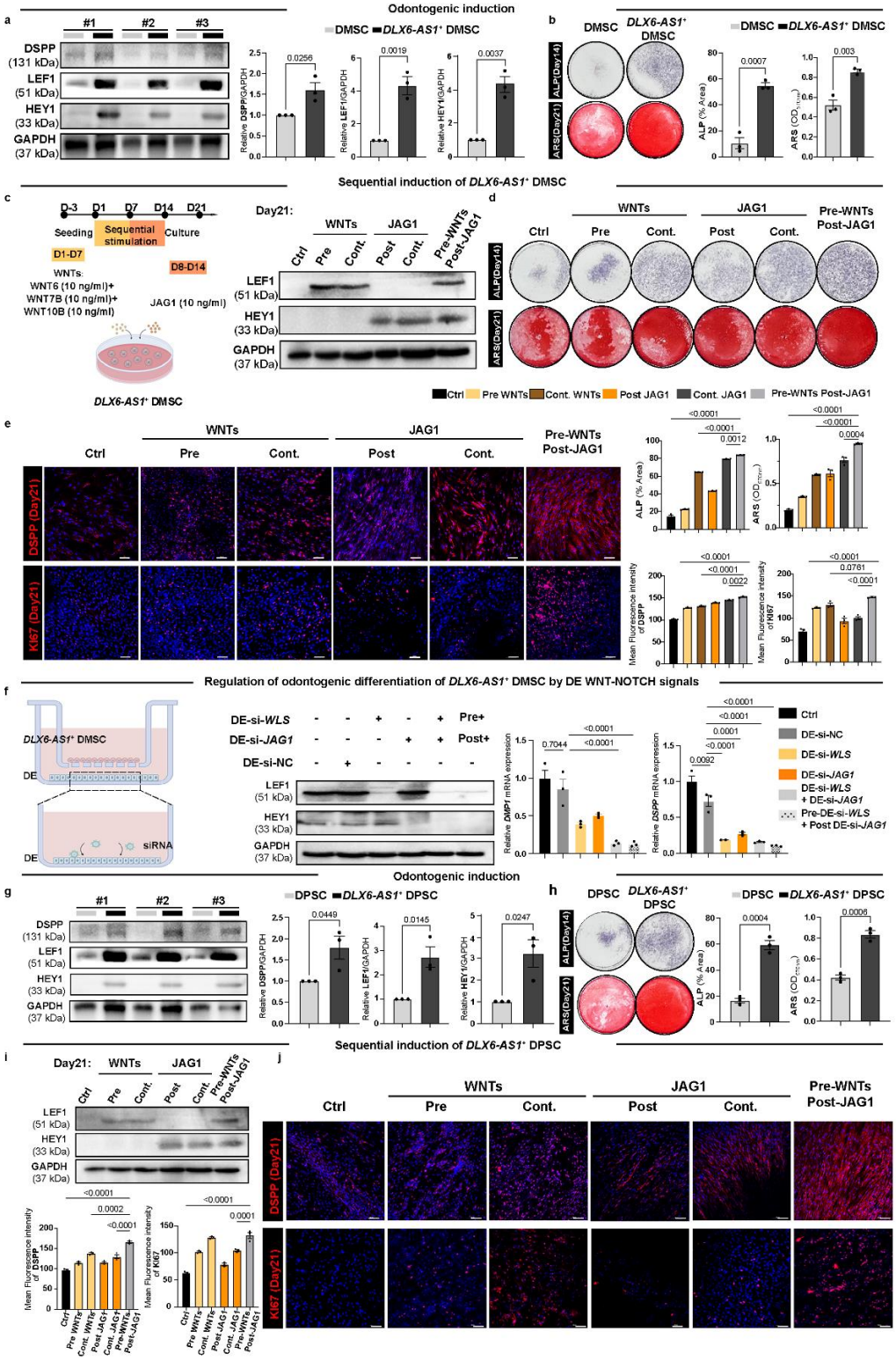


**Fig. 4. *In vitro* validation of WNT-NOTCH signal in *DLX6-AS1*$^{+}$ cells odontogenic differentiation.**

(a) Western blot analysis of DSPP, LEF1, and HEY1 in *DLX6-AS1*$^{+}$ DMSC compared to the empty vector control (DMSC).

(b) Mineralization assessment via ALP activity and Alizarin Red staining.

(c) Analysis of the protein expression of LEF1 and HEY1 in *DLX6-AS1*$^+$ DMSCs after treatment with WNTs, JAG1, or sequential WNTs-JAG1. Ctrl: *DLX6-AS1*$^+$ DMSCs that received no treatment at all (i.e., no WNTs, JAG1, or standard mineralization induction).

(d) Quantification of ALP and ARS staining in *DLX6-AS1*$^+$ DMSCs following the stimulation protocols shown in (c).

(e) IF analysis of DSPP (red) and KI67 (red) in *DLX6-AS1*$^+$ DMSCs following the stimulation protocols shown in (c). Nuclei are counterstained with DAPI (blue). Scale bars: 100 μm.

(f) Impact of epithelial *WLS* or *JAG1* knockdown on *DLX6-AS1*$^+$ DMSCs differentiation in co-culture system: protein levels of LEF1 and HEY1 by Western blot; DMP1 and DSPP expression by qPCR.

(g) Western blot analysis of DSPP, LEF1, and HEY1 in *DLX6-AS1*$^+$ DPSC compared to the empty vector control (DPSC).

(h) Mineralization evaluation through ALP activity and Alizarin Red staining.

(i) Analysis of the protein expression of LEF1 and HEY1 in *DLX6-AS1*$^+$ DPSCs after treatment with WNTs, JAG1, or sequential WNTs-JAG1. Ctrl: *DLX6-AS1*$^+$ DPSCs that received no treatment at all (i.e., no WNTs, JAG1, or standard mineralization induction).

(j) IF analysis of DSPP (red) and KI67 (red) in *DLX6-AS1*$^+$ DPSCs following the stimulation protocols in (i). Nuclei are counterstained with DAPI (blue). Scale bars: 100 μm.

All experiments were independently repeated three times with similar results; representative images are shown for blots and staining. Data in all bar graphs are presented as mean ± SEM (n=3 independent experiments). Statistical significance for two-group comparisons (a, b, g, h) was determined by a two-sided unpaired Student's t-test. For multiple-group comparisons (d, e, f, j), a one-way ANOVA followed by Tukey's multiple comparisons test was used. Exact P-values are indicated on the graphs. A P-value < 0.05 was considered statistically significant. Source data and full statistical details are provided in the Source Data file.

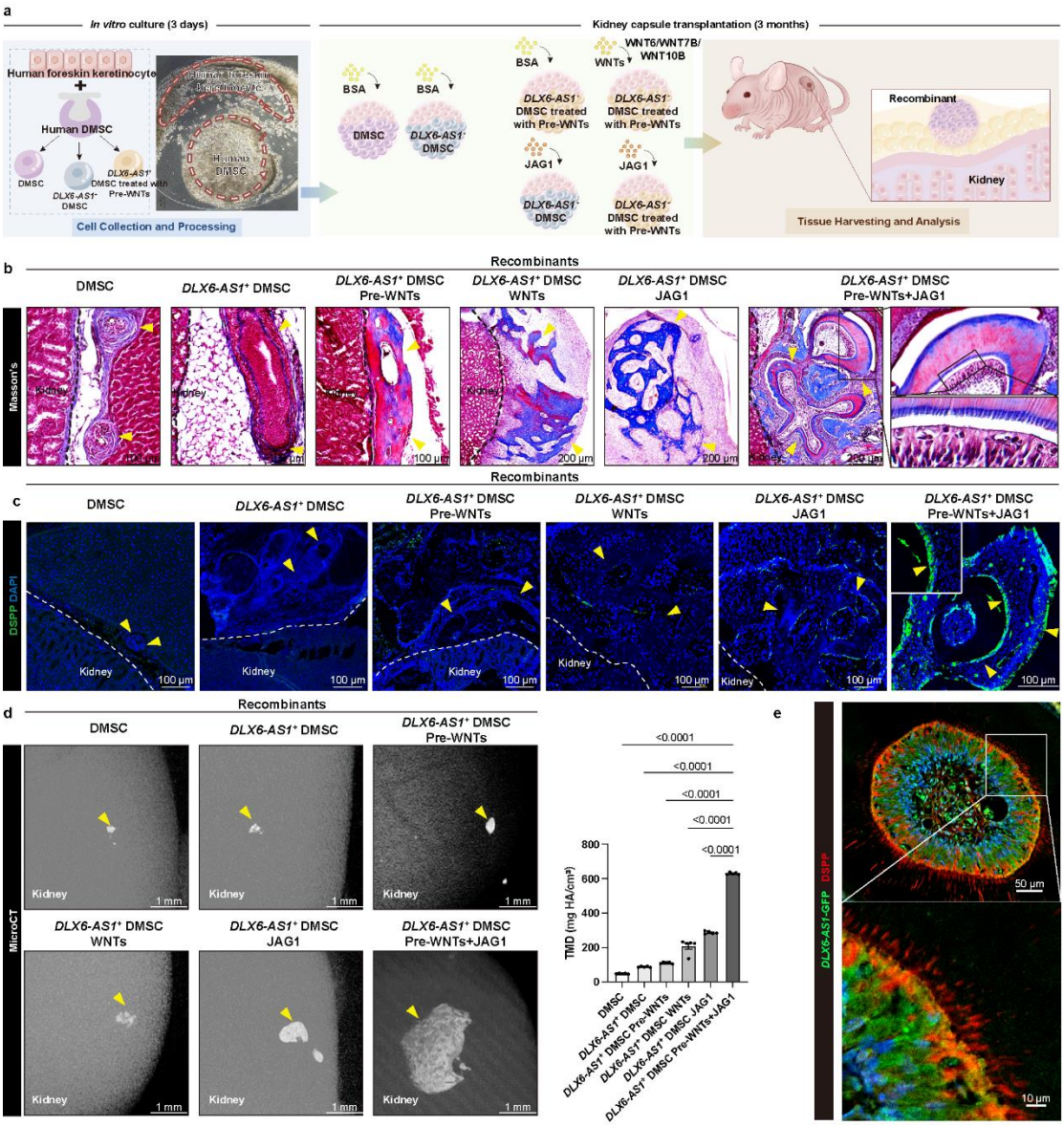


**Fig. 5. WNT-NOTCH signaling regulation of dentin formation by *DLX6-AS1*⁺ DMSCs *in vivo*.**

(a) Schematic diagram of the animal model. Renal capsule transplantation of *DLX6-AS1*⁺ DMSCs and human non-dental keratinocyte recombinants, with WNTs pretreatment and adjacent JAG1-soaked bead placement.

(b) Masson's trichrome staining analysis of retrieved recombinants. The dashed line separates the transplant from the host kidney tissue. Yellow arrowheads point to the retrieved recombinants. Scale bars in the images of the *DLX6-AS1*⁺ DMSC WNTs group, the *DLX6-AS1*⁺ DMSC JAG1 group, and the *DLX6-AS1*⁺ DMSC Pre-WNTs+JAG1 group are 200 μm, and those in other images are 100 μm.

(c) IF analysis showing the expression of the odontogenic marker DSPP (green). Nuclei were counterstained with DAPI (blue). The dashed white line separates the transplant from the host kidney tissue. Yellow arrowheads highlight DSPP-positive regions. Scale bars: 100 μm.

(d) Representative MicroCT images of mineralized tissue formation (left) and quantification of Tissue Mineral Density (TMD; right). Yellow arrowheads point to the formation of mineralized tissue. Scale bars: 1 mm. Data are presented as mean ± SEM. Statistical analysis for the multiple-group comparison was performed using a one-way ANOVA followed by Tukey's multiple comparisons test. Exact P-values are indicated on the graphs. A P-value < 0.05 was considered statistically significant.

(e) IF confirming the odontogenic differentiation of transplanted cells. *DLX6-AS1*-expressing cells, labeled with Green Fluorescent Protein (GFP; green), are shown to co-localize with the mature odontoblast marker DSPP (red). Nuclei are counterstained with DAPI (blue). Scale bars, 50 μm.

For (b-d), n=5 biologically independent samples per group were repeated with similar results. For (e), n=3 biologically independent samples per group were repeated with similar results. Representative images are shown. Source data and full statistical details are provided in the Source Data file.

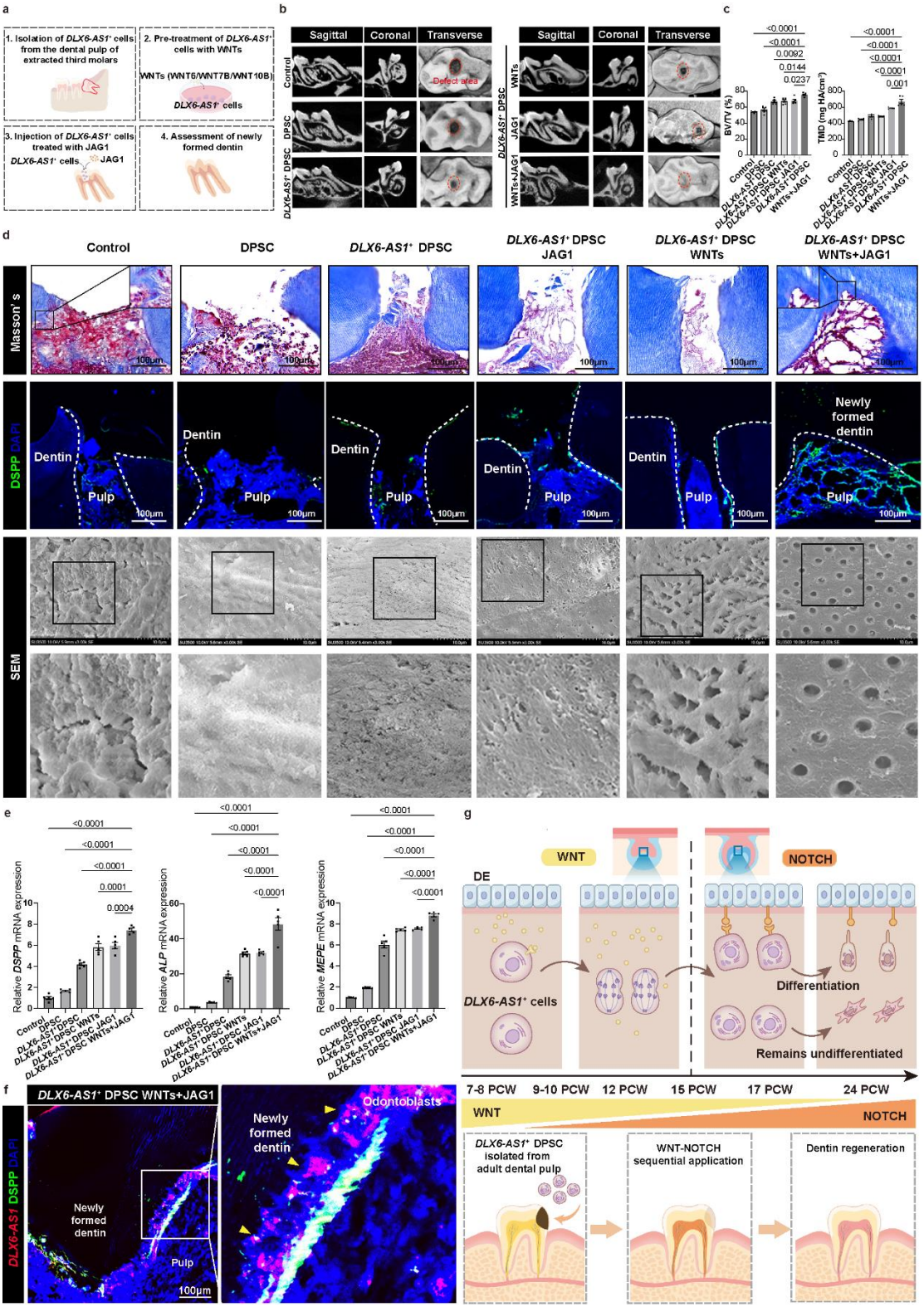


**Fig. 6. *DLX6-AS1*⁺ DPSCs-mediated dentin regeneration under WNT-NOTCH sequential activation.**

(a) Schematic diagram of the animal model. WNTs-pretreated *DLX6-AS1*$^+$ DPSCs and JAG1 delivery into exposed pulp of nude mouse molars.

(b) Representative MicroCT images (sagittal, coronal, and transverse views) showing mineralized reparative dentin formation.

(c) Quantitative assessment of bone volume fraction (BV/TV) and tissue mineral density (TMD) within damage sites. Data are presented as mean ± SEM. Statistical significance was determined using a two-sided one-way ANOVA followed by Tukey's multiple comparisons test. Exact P-values are indicated on the graphs. A P-value < 0.05 was considered statistically significant.

(d) Histological and ultrastructural analysis of the regenerated tissue. Representative images show Masson's trichrome staining, IF for DSPP (green), and SEM micrograph of the repaired site. Nuclei in IF images are counterstained with DAPI (blue). Scale bars in Masson's and IF images are 100 μm, in SEM images 10 μm.

(e) Expression of mineralization-associated genes *DSPP*, *ALP,* and *MEPE* by qPCR. Data are presented as mean ± SEM. Statistical significance was determined using a two-sided one-way ANOVA followed by Tukey's multiple comparisons test. Exact P-values are indicated on the graphs. A P-value < 0.05 was considered statistically significant.

(f) Co-localization of human *DLX6-AS1* (red) and DSPP (green) by RNA scope analysis (n=3). Nuclei are counterstained with DAPI (blue). Yellow arrowheads highlight the double-positive cells. Scale bars: 100 μm.

(g) Sequential WNT-NOTCH signaling from DE orchestrates *DLX6-AS1*$^+$ cells-mediated odontogenesis. DE-derived WNT and NOTCH signaling sequentially regulate *DLX6-AS1*$^+$ DP cells expansion and odontoblast differentiation during tooth development. This developmental paradigm enables therapeutic dentin regeneration through WNT-NOTCH sequential activation in dental pulp-derived *DLX6-AS1*$^+$ DPSCs.

For b, c, d (Masson's and IF), and e, n=5 biologically independent samples per group were repeated with similar results. For d (SEM) and f, n=3 biologically independent samples per group were repeated with similar results. Representative images are shown. Source data and full statistical details are provided in the Source Data file.

**Editor's Summary**

Here they identify key cells and signals that drive new dentin formation, enabling successful regeneration of damaged tooth structure and offering a promising dental repair strategy.

**Peer review information**: *Nature Communications* thanks the anonymous reviewers for their contribution to the peer review of this work. A peer review file is available.